[UCI]I804:24011-200000240078

August 2010

Master's Thesis

A Study on the Weldability and Mechanical Characteristics of Dissimilar Butt Joint by Laser Assisted Friction Stir Welding

Graduate School of Chosun University

Department of Naval Architecture and Ocean Engineering

Hyun-Su Kim

A Study on the Weldability and Mechanical Characteristics of Dissimilar Butt Joint by Laser Assisted Friction Stir Welding

August 2010

Graduate School of Chosun University

Department of Naval Architecture and Ocean Engineering

Hyun-Su Kim

A Study on the Weldability and Mechanical Characteristics of Dissimilar Butt Joint by Laser Assisted Friction Stir Welding

Advisor : Professor Han-Sur Bang

A Thesis submitted for the degree of
Master of Engineering

April 2010

Graduate School of Chosun University

Department of Naval Architecture and
Ocean Engineering

Hyun-Su Kim

金顯洙의 碩士學位論文을 認准함

委員長 朝鮮大學校 敎授　房　熙　善　印

委　員 朝鮮大學校 敎授　房　漢　瑞　印

委　員 朝鮮大學校 敎授　權　寧　燮　印

2010年 05月

朝鮮大學校 大學院

CONTENTS

List of Table .... Ⅳ

List of Figures .... Ⅴ

Abstract .... Ⅶ

Chapter 1. Introduction

1 . 1 Background and Purpose 1

1 . 2 Work methodology 3

1 . 3 Material used in study 5

1 . 4 Characteristics of laser assisted FSW process 6

Chapter 2. Numerical analysis for heat conduction

2 . 1 Theory of heat conduction analysis 9

2 . 2 Heat input equation 13

2 . 3 Flow chart of the FE analysis program 15

Chapter 3. Numerical analysis of Laser assisted Friction Stir Welding

3 . 1 Heat conduction analysis 17

3.1.1 Analysis model 17

3 . 2 Analysis results 21

Chapter 4. Experimental of Laser assisted Friction Stir Welding

4 . 1 Experimental work for laser assisted FSW ·········· 27

4.1.1 Laser−FSW equipment and experimental setup ····· 27

4.1.2 Description of tool material ·· 29

4 . 2 Experimental work for laser assisted FSW ·········· 30

4.2.1 Experiment to obtimum laser preheating ················· 32

4.2.2 Experiment by FSW ··· 33

4.2.3 Experiment by laser assisted FSW(LAFSW) ········· 36

4 . 3 Tensile test resultst ·· 45

4.3.1 Tensile test ·· 45

4.3.2 Tensile test for similar joint(Al6061−T6) ············ 46

4.3.3 Tensile test of FSW dissimilar joint ························ 47

4.3.4 Tensile test of laser assisted FSW dissimilar joint ··· 50

4 . 4 Hardness test results ·· 56

4.4.1 Hardness test ··· 56

4.4.2 Hardness result ·· 57

4 . 5 Microstructure analysis of dissimilar joint ············ 59

4.5.1 Microstructure analysis ·· 59

4.5.2 Microstructure of FSW dissimilar joint ···················· 60

4.5.3 Microstructure of laser assisted FSW dissimilar joint ··· 62

4 . 6 Analysis of weld specimen using SEM and EDS observation ········· 64
4.6.1 SEM of fractured specimens ········· 64
4.6.2 SEM and EDS observation of dissimilar joint by LAFSW ········· 67
Chapter 5. Conclusion ········· 70
Reference ········· 72

List of Tables

Table 1.1 Chemical compositions in Al6061-T6 and SS400 5
Table 1.2 Mechanical properties of Al6061-T6 and SS400 5
Table 4.1 Chemical composition and mechanical properties of tool 29
Table 4.2 Conditions for laser preheating 32
Table 4.3 FSW parameters 34
Table 4.4 Bead shapes of FSW weldment 35
Table 4.5 LAFSW parameters 37
Table 4.6 Bead shapes of LAFSW weldment 40
Table 4.7 Tensile test specimen dimensions 45
Table 4.8 Tensile tested similar joint 46
Table 4.9 Fractured specimens and cross sections of dissimilar joint by FSW 48
Table 4.10 Stress-strain curve for dissimilar weld joint by FSW 49
Table 4.11 Fractured specimens and cross sections of dissimilar joint by laser assisted FSW 51
Table 4.12 Stress-strain curve of dissimilar weld joint by LAFSW 53

List of Figures

Fig. 1.1 Application of Friction Stir Welding in industries 2
Fig. 1.2 Typical model of the data transferring 3
Fig. 1.3 Schematic of Laser assisted Friction Stir Welding 8
Fig. 1.4 Characteristics of FSW joint 8
Fig. 2.1 Flow chart of the heat transfer analysis program 16
Fig. 3.1 Model for numerical analysis 18
Fig. 3.2 Temperature dependent mechanical properties of Al6061−T6 18
Fig. 3.3 Temperature dependent mechanical properties of SS400 19
Fig. 3.4 Mesh division for FEM analysis 20
Fig. 3.5 Heat distribution contour in the model by FSW 23
Fig. 3.6 Heat distribution contour in the model by laser assisted FSW 24
Fig. 3.7 Temperature history of laser assisted FSW−Aluminum side .. 25
Fig. 3.8 Temperature history of laser assisted FSW−Steel side 26
Fig. 4.1 Specifications of equipment 28
Fig. 4.2 Experimental set−up for laser assisted FSW joint 28
Fig. 4.3 Dimensions and shape of tool 29
Fig. 4.4 Schematic diagram and welding parameters of LAFSW 31
Fig. 4.5 Schematic of laser and tool position 31
Fig. 4.6 Tensile test specimen details 45
Fig. 4.7 Rotation speed versus tensile strength 55
Fig. 4.8 Vickers hardness test machine and specimen 56
Fig. 4.9 Vickers hardness test machine and specimen 56
Fig. 4.10 Hardness testing result of LAFSW 58

Fig. 4.11 Hardness testing result of FSW and LAFSW ······························ 58
Fig. 4.12 Optical microscope ·· 59
Fig. 4.13 Microstructural (FSW) ··· 61
Fig. 4.14 Microstructural (LAFSW) ··· 63
Fig. 4.15 SEM of dissimilar joint by FSW ··· 65
Fig.4.16 SEM of dissimilar joint by LAFSW ·· 66
Fig 4.17. SEM of LAFSW ·· 67
Fig 4.18. EDS of Al6061 by LAFSW ·· 68
Fig 4.19. EDS of SS400 by LAFSW ··· 69

ABSTRACT

Laser-FSW Hybrid 접합기술을 적용한 이종재료(Al6061/SS400) 접합부의 접합성 및 기계적 특성에 관한 연구

Kim, Hyun-Su
Advisor : Prof. Bang, Han-sur, Ph.D.
Department of Naval Architecture and Ocean Engineering ,
Graduate School of Chosun University

범세계적으로 강력해진 환경규제로 인하여 21세기를 맞이한 현대사회의 각종산업분야에서 최대의 핵심 과제는 “환경과의 조화-녹색성장”일 것이다. 이에 이산화탄소 증가로 인한 지구온난화는 심각한 문제로 지적되고 있다. 이러한 국제적 규제의 대응 및 문제 해결 방안으로 철도차량, 자동차, 선박, 항공기 등의 수송기계분야에 있어서는 이산화탄소 배출의 삭감에 기여하는 기술로서 엔진효율 및 연소방식의 개선, 수송기계의 중량저감, 동력전달의 효율화 등이 개발 및 적용되어지고 있다. 특히, 수송기계 차제의 중량은 연비 및 이산화탄소 배출에 직접적인 영향을 미치고 있어 차제에 경량 소재재료들의 적용에 대한 요구 및 관심이 빠르게 증가되고 있는 실정이다.

경량금속인 알루미늄의 경우 비중이 강의 1/3로서 낮은 밀도에도 불구하고, 비강도가 높고, 특히 각종 원소와의 결합을 통한 합금성이 우수하다. 또한, 소성가공성이 좋고 전기전도도 및 대기중에 내식성과 내마모성이 우수하여 구조 및 기능성금속으로서 다른 경향 소재에 비해 적용범위 및 활용도가 높은 비철재료이다. 하지만 기존의 용융용접방법으로는 고온균열 감수성이 높은 알루미늄 합금을 용접하는 경우 균열 및 기공의 발생 등으로 용접에 어려운 점이 많다.

이러한 문제점 등을 개선한 접합방법으로 마찰교반접합(FSW)기술이 적용되어지고 있다. 이 기술은 회전하는 Tool을 피접합체에 삽입하여 마찰발열에

의해 접합체를 연화시켜 소성유동을 통해 접합하는 비소모성 접합방법으로서 알루미늄 합금의 경우 고상접합이므로 용융용접에서 생길 수 있는 균열(액화균열, 응고균열)및 합금원소의 손실을 방지할 수 있고, 접합부의 결정립 미세화 등의 고품질 접합부를 얻을 수 있는 환경친화형 접합방법이다.

더불어 보다 효과적인 수송기계 분야의 강도 확보 및 경량화를 위해서는 이종소재(알루미늄 합금과 스틸) 접합을 통한 경량화 추진이 필요하나, 스틸과 알루미늄 합금의 이종소재 접합기술의 부재로 국내외 산업응용분야에서의 실제구현은 거의 이루어지지 않고 있다.

또한 알루미늄합금의 경우 강에 대비하여 열전도도는 4배, 선팽창계수는 약 2배, 응고수축률은 1.5배로서 이러한 물리적 특성이 상이한 이종재료(Al 6061, SS400)간에 기존의 접합방법으로 리벳팅 및 바이메탈을 이용한 용융용접을 적용하였으나 이에 소요 공정 시간의 증가 및 용접열에 의한 용접결함(변형, 잔류응력, 응고균열, 기공, 산화 등) 뿐만 아니라 금속간 화합물생성으로, 접합부의 강도저하로 건전한 접합부를 얻기가 어렵다.

따라서 본 연구는 저밀도 이면서 비강도가 우수한 알루미늄 합금(Al6061)과 일반 구조용압연강재로 우수한 가공성 및 강도를 지닌 Mild Steel(SS400) 이종재료에 Nd:YAG Pulse Laser(600W)와 FSW를 결합한 Hybrid 접합기술을 적용하여 접합을 수행하였으며, 아울러 기계적 특성(인장시험. 경도시험) 및 금속학적 특성(광학현미경, SEM, EDS)을 파악하여 이종재료의 접합성을 평가하고 수송기계 분야의 적용성을 고찰하고자 한다.

Chapter 1

INTRODUCTION

1.1 Background and purpose

The need of reducing light weight products is increasing day by day , especially in vehicle manufacturing industry. Today, the whole world is continuously tightening emission restrictions both on land and at sea for which a solution is light weight structures. Recently, researchers are focusing on fabricating light weight structures which are economical and environmentally friendly. Outstanding properties of aluminum such as, lightweight, corrosion-resistant etc, opens up a whole new world of design possibilities for engineering and architecture professionals to meet design goals. Combining aluminum alloys with whole products is expensive and also there is limitations in making required shapes.

Dissimilar joints are used in structures where light weight and high strength are desirable. Riveting, and bimetallic strip joining techniques for dissimilar material joint increases manufacturing cost and require more man hours. However, welding aluminum alloys to steel with classical fusion welding techniques is generally difficult due to the wide differences in their thermal and mechanical properties, and the tendency to form hard and brittle inter-metallic compounds such as Fe_2Al_5 and $FeAl_3$. Solid state bonding method like Friction Stir Welding (FSW) offers substantial advantages over friction welding and diffusion bonding and is potentially a practicable joining process for dissimilar materials.

Joining dissimilar materials, especially steel to aluminum, by FSW requires high tool load and equipment rigidity. In addition, the weld material get red hot and the wear debris from the tool can frequently be found inside the weld. In laser welding of steel to aluminum the possibility of intermetallic compounds to appear in the weld is more producing poor welds. To overcome this problem for joining dissimilar joint, laser preheating can be implemented. Hence, this work intends to establish the possibility of joining dissimilar joint (Al6061-T6 & SS400) by Laser assisted FSW(LAFSW). For this, weldability, thermal characteristics, mechanical characteristics and metallurgical characteristics of dissimilar joint by LAFSW is studied. Successfully obtaining the process of dissimilar metal joining by LAFSW and analysis of the experimental data influence the industrial and national competitiveness.

Scientifically, this method could be a basic of another dissimilar metal joining following this study. Finally, this study contributes to industries world wide who looks forward to decline trial and error methods, improve their own competitiveness in that field.

Fig. 1.1 Application of Friction Stir Welding in industries

1.2 Work methodology

The work methodology followed for this work are as follows:

1) Numerical analysis for heat conduction

The analysis of heat conduction is carried out using inhouse solver and the thermal characteristics of dissimilar joint by Laser assisted FSW was studied. The equation of non-stationary heat conduction is adopted and the heat conduction in solid material is formulated by finite element method using Galerkin method, and the Iso-parametric element is used for analysis. Temperature dependence of specific heat, coefficient of heat transfer, thermal conduction and density were considered assuming the material to be isotropic. The convective and radiation heat transfer is not considered for the analysis. Heat input is given to the developed heat input model considering the coefficient of friction and slip.

The data transfer flow diagram used for numerical analysis is as shown in Fig 1.2

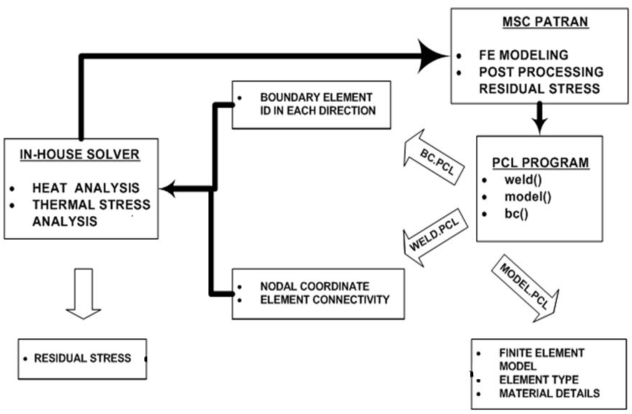

Fig. 1.2 Typical model of the data transferring

2) FSW experiment on dissimilar materials to find optimum welding conditions.

In experiments, 90 trials has been carried out to obtain optimum welding condition by Friction Stir Welding. Tilt angle, tool geometry, thickness, room temperature were fixed and tool travel speed and tool rotation speed were changed.

3) Laser assisted FSW on dissimilar materials to find optimum welding conditions

Considering the optimum conditions obtained from FSW experiments laser preheating on steel side was carried out. The laser focus distance and shielding gas composition was varied to obtain the optimum welding condition.

4) Mechanical tests and microstructural analysis

Mechanical tests were carried out to test the weld strength of dissimilar joint and the microstructural analysis were carried out to study the change in microstructure on TMAZ, HAZ, and SZ and compared with base metal using SEM data and EDS.

5) Comparison of numerical simulation result with experiment(infra red camera).

Thermal camera was used to measure the temperature at the tool-work piece. The thermal camera result was used to compare with the numerical simulation results.

1.3 Material used in study

The materials used for this study are Al6061-T6 and SS400. To minimize the mechanical effect in welds such as contraction and expansion in weldment, specimens with dimension 200×100×3mm was made to conduct the welding experiment. Chemical composition and mechanical proerties of base metals are given in Table 1.1 and 1.2 respectively.

Table 1.1 Chemical compositions in Al6061-T6 and SS400

Material	Chemical Composition (Wt%)								
Al6061-T6	Si	Fe	Cu	Mn	Mg	Cr	Ni	Zn	Ti
	0.70	0.64	0.28	0.08	0.37	0.19	0.01	0.05	0.05
SS400	C	Si	Mn	P	S				
	0.1438	0.009	0.664	0.012	0.0039				

Table 1.2 Mechanical properties of Al6061-T6 and SS400

Material	Y.S(MPa)	T.S(MPa)	E.I(%)
Al6061-T6	300	330	13
SS400	312	450	37

Al6061-T6 has good mechanical properties and exhibits good weldability.

Steel SS400 is a kind of new steel with superfine grain and super purity, and has an excellent mechanical property. SS400 have excellent weldability, good machinability, superior operational performance and very cheap. Study of welding structure characteristics is essential for its promotion and application.

Al6061-T6 is widely used for construction of aircraft structures, yacht construction, including small utility boats, automotive parts etc.

SS400 is widely used in shipbuilding applications and other application includes floor boards, deck boards, factory stair boards, car boards, lorry beds, elevator floor and general fabrication.

1.4 Characteristics of Laser assisted FSW process

Friction Stir Welding(FSW) was invented at the TWI in 1991 as a solid state joining technique and was initially applied to Al alloy. the basic concept of FSW is remarkably simple. A nonconsumable rotating tool with a specially designed pin and shoulder is inserted in to the abutting edges of sheet or plates to be joined and subsequently traversed along the joint line. Fig. 1.3 illustrates process definition for the tool and workpiece. The tool serves three primary function, that is, heating of the workpiece, movement of material to produce the joint, and containment of hot metal beneath the tool shoulder. Heating is created within the workpiece both by friction between the rotating tool pin and shoulder and by severe plastic deformation of the workpiece. The localized heating softens material around the pin and, combined with the tool rotation and translation, lead to movement of material from the front to the back of the pin, thus filling the hole in the tool wake as the tool moves forward. The tool shoulder restricts metal flow to a level equivalent to the shoulder position, that is, approximately to the initial workpiece top surface.

As a result of the tool action and influence on the workpiece, when performed properly, a solid-state joint is produced, that is, no melting. Because of various geometrical features on the tool, material movement around the pin can be complex, with gradients in strain, temperature, and strain rate. Accordingly, the resulting stir zone microstructure reflects thes different thermomechanical histories and is not homogeneous. In spite of the local microstructural in homogeneity, one of the significant benefit of solid-state welding technique is the fully recrystallized, equiaxed, fine grain microstructure created in the nugget by the intense plastic deformation at evaluated temperature

◎ FSW has many advantages, including the following:

• The welding procedure is relatively simple with no consumables of filler metal.
• Joint edge preparation is not needed
• The procedure can be automated and carried out in all positions.
• High joint strength has bees achieved
• FSW can be used with alloys that cannot be fusion welded due to crack sensitivity

◎ Drawbacks of FSW, including the following:

• FSW needed for powerful fixtures to clamp the workpiece to welding table.
• The high force needed to move the welding tool forward
• The relatively high wear rate of the welding tool

To overcome these drawback, a laser-assisted friction stir welding system has been developed. the system combines a conventional commercial milling machine and Nd:YAG laser system. Laser power is used to preheat the workpiece at a localized area ahead of the rotating tool, thus plasticizing a volume of the work piece ahead of the tool. The work piece is then joined in the same way as in the conventional FSW process. The high temperature ahead of the rotating tool softens the workpiece and enables joining with out strong clamping fixtures. Less force is needed to move the welding tool forward, hence, wear is reduced. A further advantage of laser energy for this process is ability to weld at higher rates without causing excessive wear to the welding tool.

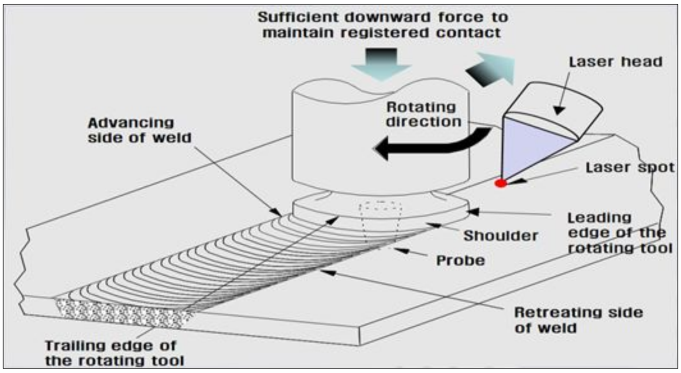

Fig. 1.3 Schematic of Laser assisted Friction Stir Welding

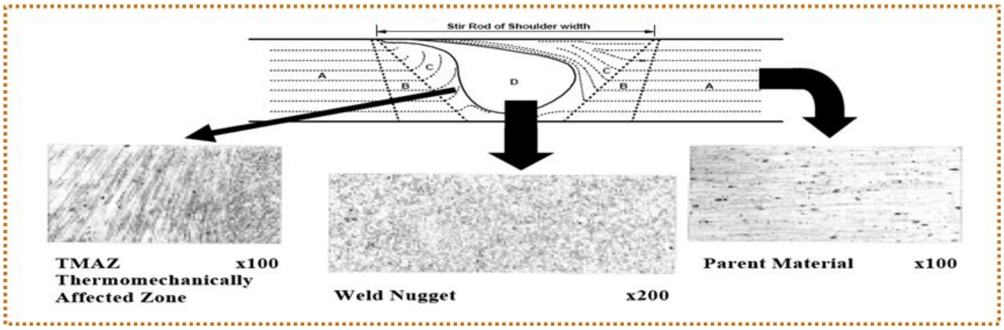

A. BM(Base Metal)

B. HAZ(Heat Affected Zone; affected by heat generated during FSW)

C. TMAZ (Thermomechanically Affected Zone)

: contains material that interacts indirectly with the tool , plastically deformed with partial recrystallization

D. SZ(Stir Zone)

:contains material that interacts directly with the tool, dynamically recrystallized)

Fig. 1.4 Characteristics of FSW joint

Chapter 2
Numerical analysis for heat conduction

There ara many practical engineering problems that require the analysis of heat transfer. In this paper, the finite element codes for the heat transfer analysis of dissimilar material welding, between aluminum alloy(Al6061-T6) and Steel(SS400), has been developed. In many case, a significant percentage of the time spent on FEM analysis is for pre- and post processing. This is common for numerous FEM code used in specialized researches. In the present work, an interface has been developed using the high level language PCL(PATRAN Command Language) that can be complied directly from PATRAN desktop so that PATRAN can be used as pre- and post processor for the developed FEM.

2.1 Theory of heat conduction analysis

The spatial and temporal temperature distribution satisfies the following governing equation of un-stationary heat conduction:

$$\rho c \frac{\partial T}{\partial t} = \lambda \left(\frac{\partial^2 T}{\partial x^2} + \frac{\partial^2 T}{\partial y^2} + \frac{\partial^2 T}{\partial z^2} \right) + \dot{Q} \tag{2.1}$$

where T is temperature(℃), ρ is density(g/cm3), $\dot{Q}$ is rate of temperature change due to heat generation per volume (cal/cm3·sec), t is time (sec), λ is thermal conductivity of isotropic material (cal/cm·sec·℃) and c is specific heat (cal/g·℃).

Heat conduction problem for the object of analysis is formulated as the finite element method using Galerkin method.

Internal temperature of the element, T , is given by

$$T(x,y,z,t) = [N(x,y,z)]\{\phi(t)\} \quad (2.2)$$

where $[N]$ is a shape function matrix shown the relation between nodal temperature and internal temperature of the element. $\{\phi\}$ is the vector of the nodal temperature of the element at time t .

If Galerkin method is applied in Equation (2.1) using $[N]$ as a weighting function at this time, following equation is obtained.

$$\int_{V^e} [N]^T \left\{ \lambda\left(\frac{\partial^2 T}{\partial x^2} + \frac{\partial^2 T}{\partial y^2} + \frac{\partial^2 T}{\partial z^2}\right) + \dot{Q} - \rho c \frac{\partial T}{\partial t} \right\} dV = 0 \quad (2.3)$$

where superscript, T ,shows transformation of matrix and subscript, V^e , shows the domain of element.

Un-stationary heat conduction problem can be expressed as following finite element expression for an element.

$$[k]\{\phi\} + [c]\left\{\frac{\partial \phi}{\partial t}\right\} = \{f\} \quad (2.4)$$

where $[k]$, $[c]$ and $\{f\}$ show the heat conductivity matrix of an element, the heat capacity matrix of an element and the heat flow vector of an element, respectively. They are expressed as follows:

$$[k]=\int_{V^e}\lambda\left(\frac{\partial[N]^T}{\partial x}\frac{\partial[N]}{\partial x}+\frac{\partial[N]^T}{\partial y}\frac{\partial[N]}{\partial y}+\frac{\partial[N]^T}{\partial z}\frac{\partial[N]}{\partial z}\right)dV \quad (2.5)$$

$$[c]=\int_{V^e}\rho c[N]^T[N]dV \quad (2.6)$$

$$\{f\}=\int_{V^e}\dot{Q}[N]^T dV-\int_{S^e}q[N]^T dS \quad (2.7)$$

Boundary conditions on the boundary S_2 to S_4 can be given to substitute q in second term of equation (2.7).

- When the heat flux, q_o ,flows from the boundary S_2 :

$$\int_{S_2^e}q[N]^T dS=\int_{S_2^e}q_o[N]^T dS \quad (2.8)$$

- When heat transfer is on the boundary S_3 for convection:

$$\int_{S_3^e}q[N]^T dS=\int_{S_3^e}\alpha_c(T-T_c)[N]^T dS \quad (2.9)$$

If T in the equation(2.9) is substituted, the equation(2.10) becomes as follows:

$$\int_{S_3^e}q[N]^T dS=\int_{S_3^e}\alpha_c[N]^T[N]dS\cdot\{\phi(t)\}-\int_{S_3^e}\alpha_c T_c[N]^T dS \quad (2.10)$$

- When heat radiation is on the boundary S_4 :

$$\int_{S_4^e}q[N]^T dS=\int_{S_4^e}\alpha_r(T-T_r)[N]^T dS \quad (2.11)$$

If T in the equation(2.11) is substituted by the equation(2.2), The equation(2.12) becomes as follows:

$$\int_{S_4^e} q[N]^T dS = \int_{S_4^e} \alpha_r [N]^T [N] dS \cdot \{\phi(t)\} - \int_{S_4^e} \alpha_r T_r [N]^T dS \tag{2.12}$$

$$[k] = \int_{V^e} \lambda\left(\frac{\partial[N]^T}{\partial x}\frac{\partial[N]}{\partial x} + \frac{\partial[N]^T}{\partial y}\frac{\partial[N]}{\partial y} + \frac{\partial[N]^T}{\partial z}\frac{\partial[N]}{\partial z}\right) dV$$

$$+ \int_{S_3^e} \alpha_c [N]^T [N] dS + \int_{S_4^e} \alpha_r [N]^T [N] dS \tag{2.13}$$

$$\{f\} = \int_{V^e} \dot{Q} [N]^T dV - \int_{S_2^e} q_0 [N]^T dS$$

$$+ \int_{S_3^e} \alpha_c T_c [N]^T dS + \int_{S_4^e} \alpha_r T_r [N]^T dS \tag{2.14}$$

Therefore, finite element formula of an element can be derived as a form of matrix equation including boundary conditions by using equation (2.6), (2.13) and (2.14).

Finite element formula for the whole object analyzed is constructed with assembled each matrix of elements and it can be expressed as follows:

$$[K]\{\Phi\} + [C]\left\{\frac{\partial \Phi}{\partial t}\right\} = \{F\} \tag{2.15}$$

where $[\Phi]$, $[K]$, $[C]$ and $\{F\}$ show the vector of the nodal temperature in the whole object, the heat conductivity matrix in the whole object, the heat capacity matrix in the whole object and the heat flow vector in the whole object, respectively. They are given as follows.

$$[\Phi]=\sum_e \phi \quad , \quad [K]=\sum_e k \quad , \quad [C]=\sum_e c \quad , \quad \{F\}=\sum_e f \qquad (2.16)$$

2.2 Heat input equation

The total heat generation in FSW is due to tool-workpiece friction and viscous dissipation. Previous studies reports the heat generated due to viscous dissipation is only 4% of the total heat generation. Therfore in this study, for heat conduction analysis, heat due to viscous dissipation is not considered. Many researches reports that tool shoulder contributes major part of heat generation in FSW when compared to heat at tool side and tool bottom. The total heat generated in FSW is given by;

$$Q_{total}=Q_{shoulder}+Q_{pinbottom}+Q_{pinsurface} \qquad (2.17)$$

where $Q_{shoulder}$, $Q_{pinsurface}$ and $Q_{pinbottom}$ are the total heat generated at the shoulder, pin surface and pin bottom respectively.

The heat energy at shoulder, pin bottom and pin surface per unit length is given by

$$Q_{shoulder}=\left[\frac{2}{3}\pi(\delta\tau_{yield}+(1-\delta)\mu p)\times\omega(R_s^3-R_1^3)\right]\div W_s \qquad (2.18)$$

$$Q_{pinsurface}=\left[\frac{2}{3}\pi(\delta\tau_{yield}+(1-\delta)\mu p)\times\omega\times 3R_2^2 H\right]\div W_s \qquad (2.19)$$

$$Q_{pinbottom} = \left[\frac{2}{3}\pi(\delta\tau_{yield} + (1-\delta)\mu p) \times \omega \times R_2^3 \right] \div W_s \tag{2.20}$$

R_s is the shoulder radius (mm)

R_1 is the pin radius at shoulder side (mm)

R_2 is the pin bottom radius (mm)

H is the height of the pin (mm)

P is the contact pressure (MPa)

τ_{yield} is the yield shear stress of the material at maximum temperature (MPa)

ω is tool angular rotation speed in rad/sec

μ friction coefficient

δ contact state variable (slip)

W_s is the welding speed (mm/sec)

The heat flux (Cal/mm^2.sec) for heat input elements is given by

$$q = \frac{Heat\ energy\ per\ unit\ length\ of\ weld \times Weld\ length}{No.\ of\ element \times Area\ of\ element \times Time} \tag{2.21}$$

2.3 Flow chart of the FE analysis program

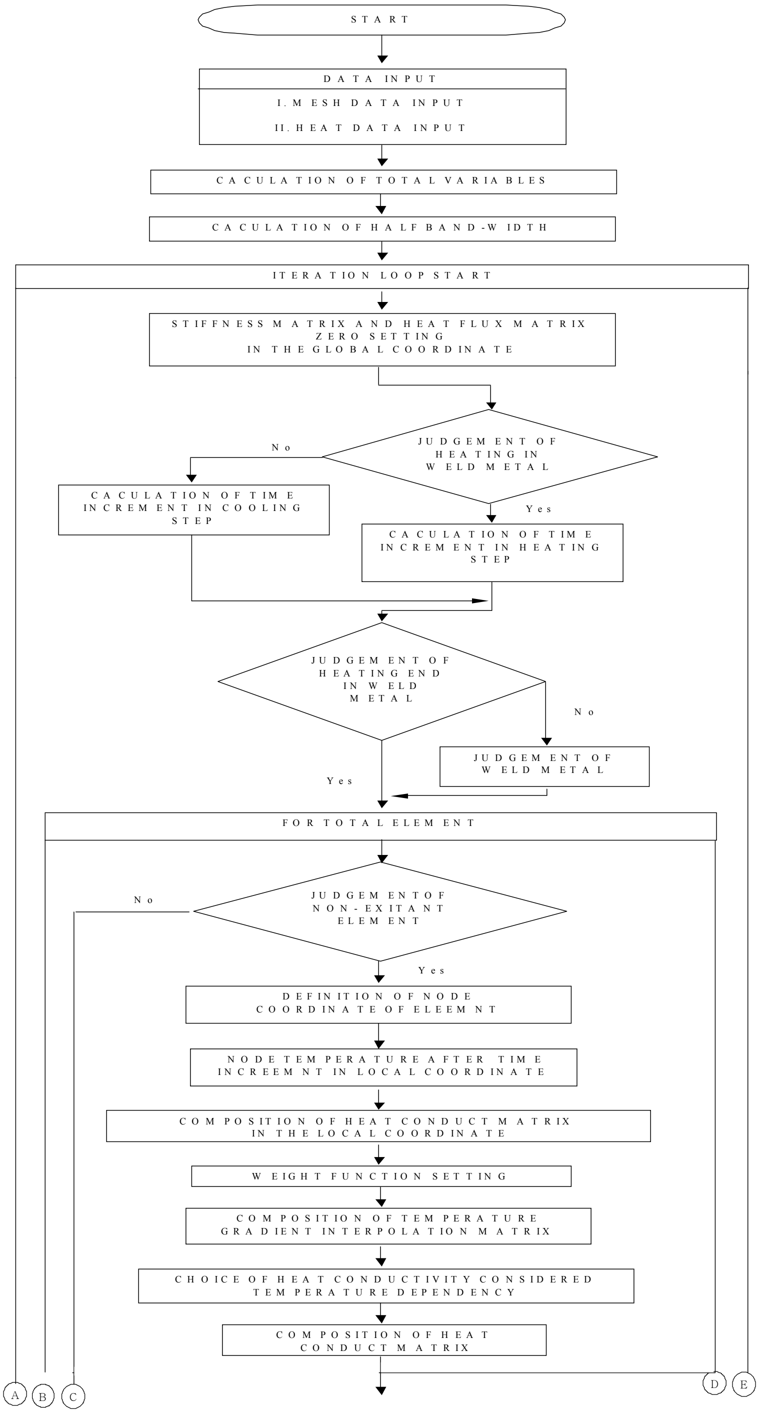

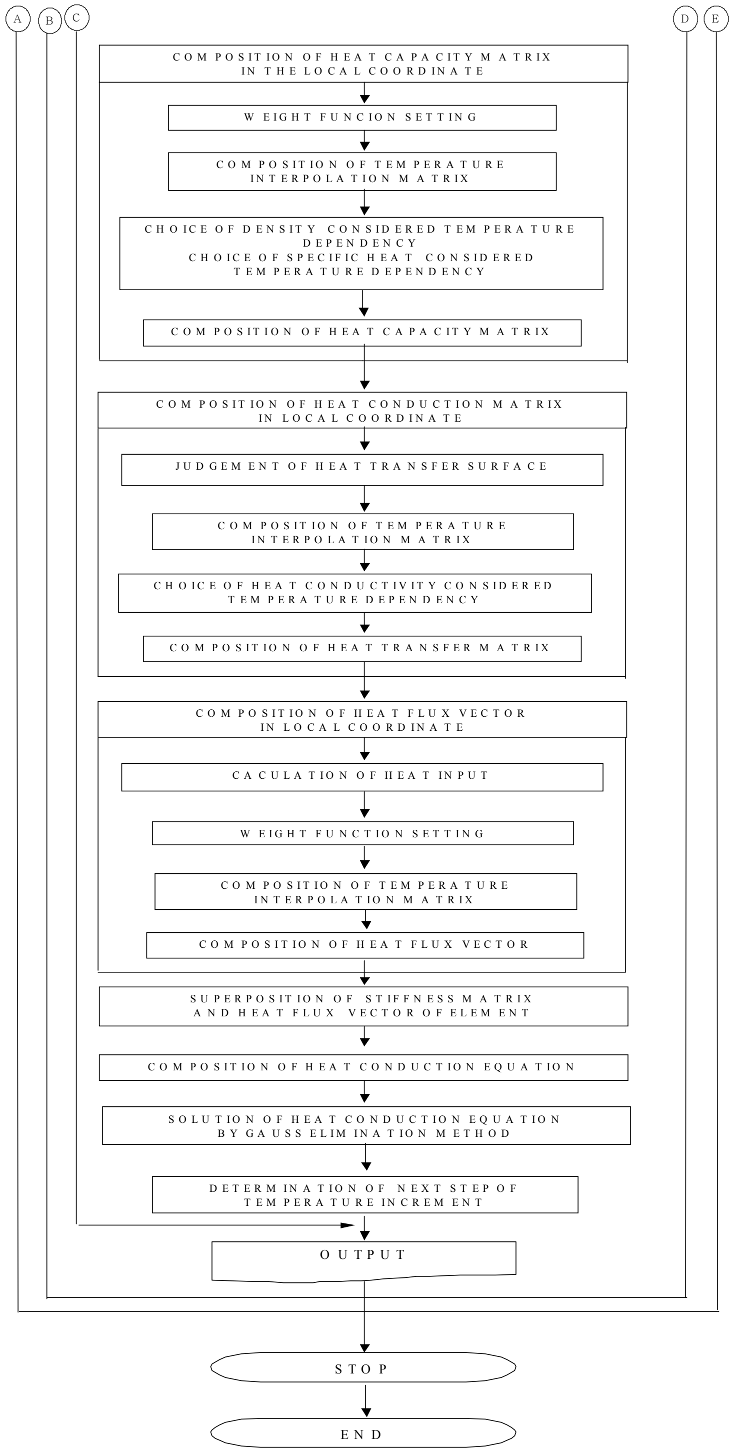

Fig. 2.1 Flow chart of the heat transfer analysis program

Chapter 3

Numerical analysis of Laser assisted Friction Stir Welding

3.1 Heat conduction analysis

Thermal distribution numerical analysis was carried out to examine closely the thermal characteristics occurring in dissimilar joint(Al6061-T6/SS400) by Laser assisted FSW.

In order to analyze the thermal distribution precisely, the theory of non-stationary thermal conduction was adopted considering temperature dependent material properties. A computer program for numerical analysis was developed using iso-parametric element, after formulating the adopted theory into finite element formula. By using this developed program, it is intended to carry out the numerical simulation to the dissimilar weldment (Al6061-T6/SS400) and examine the thermal characteristics.

Numerical analysis model was developed as per the weld geometry and optimized welding condition obtained from experiment.

3.1.1 Analysis model

As shown in Fig.3.1, The minimum dimension of dissimilar (Al6061-T6/SS400) specimen (100×200×3) was selected as in experiment to minimize the mechanical effect in welds such as contraction and expansion in weldment.

To analyse the temperature distribution in welded plate, x-axis is placed in transverse direction of welding, the y-axis is placed along the thickness of the weldment, and the z-axis lies in the direction of welding.

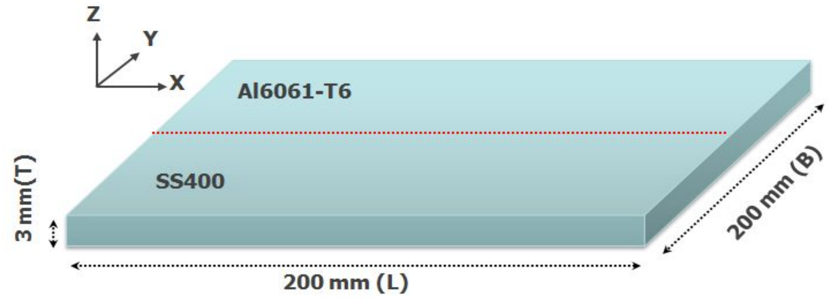

Material	L (mm)	B (mm)	T (mm)
Al6061-T6	200	100	3
SS400	200	100	3

Fig. 3.1 Model for numerical analysis

Temperature dependent material properties of Al6061-T6 and SS400 considered for finite element analysis of dissimilar material welded model are given in Fig. 3.2 and Fig. 3.3.

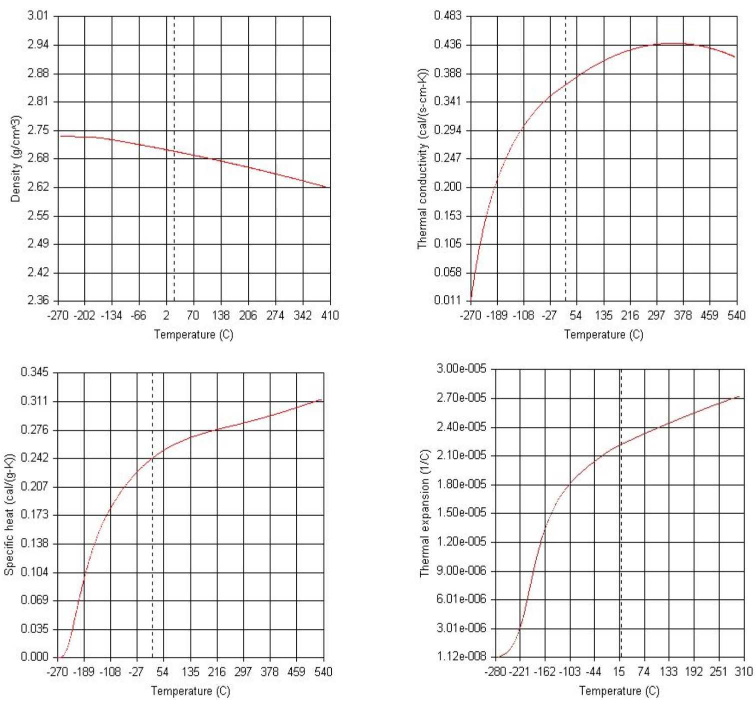

Fig. 3.2 Temperature dependent mechanical properties of Al6061-T6

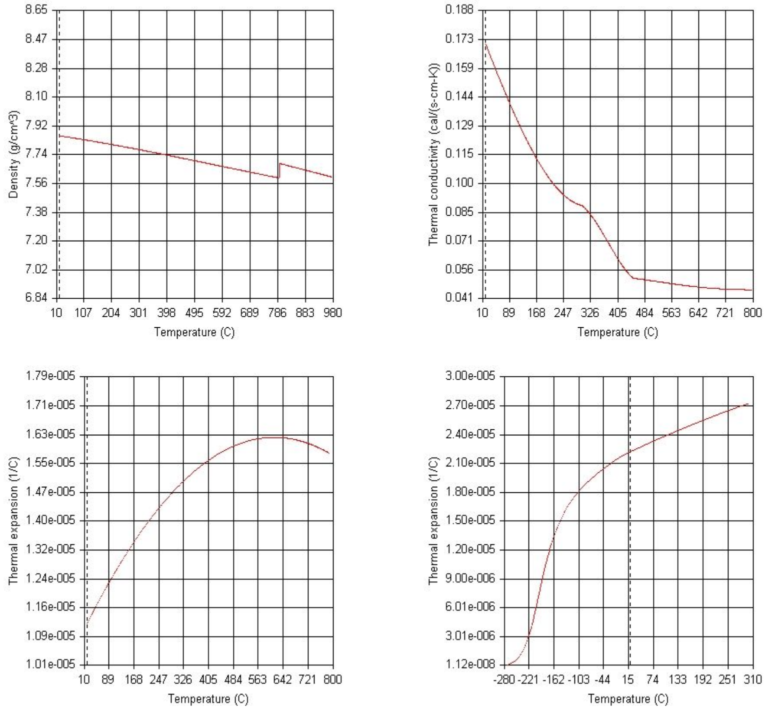

Fig. 3.3 Temperature dependent mechanical properties of SS400

The mesh division for heat conduction analysis is as shown in Fig 3.4. To obtain more accurate results, the mesh size is chosen finer at and near weld area compare with other regions. The tool area element are considered as non-existent for this analysis and therefore the tool side elements are eliminated. Total number of elements and nodes are 3570 and 3824 respectively.

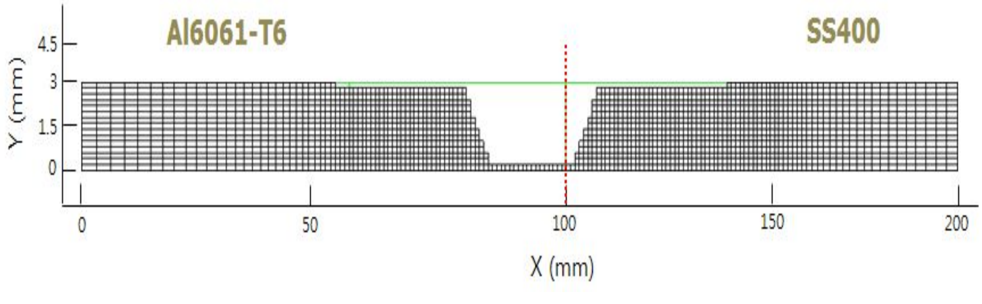

(a) Mesh division

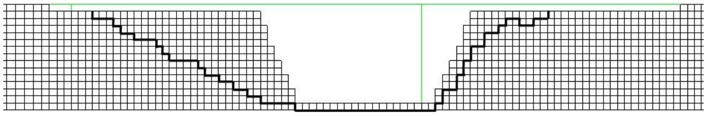

(b) Heat given elements

Fig. 3.4 Mesh division for FEM analysis

For LAFSW analysis of butt welded joint, total heat input (Eqn 3.1) is considered at laser affected area elements.

$$Q_{total} = Q_{FSW} + Q_{Laser} \tag{3.1}$$

$$Q_{Laser} = \eta_L \times \frac{P_{Laser}}{W_S} \tag{3.2}$$

Where P_{Laser} is beam power of laser at workpiece, W_S is welding speed, and η_L is the heat transfer efficiency of laser.

3.2 Analysis results

The temperature distribution from two dimensional analysis were investigated for FSW and LAFSW and is given in Fig 3.5 and 3.6 respectively. The temperature fields obtained for FSW at 0.05, 0.71, 1.21and 6.42 seconds and temperature fields obtained for LAFSW at 0.05, 0.71, 1.21and 8.39 seconds are shown respectively.

From the analysis results of FSW simulation, at 0.71second the maximum temperatures obtained at SS400 side and Al6061 are 649.81°C and 422.34°C respectively. As time passes, gradual cooling take place at steel side, but at the same time the temperature is found increasing in Al6061 tool bottom than its shoulder bottom and tool surface. ie, at 1.21 second, the temperature at shoulder bottom and tool bottom is found 416.9°C and 433°C at Al6061 side. The temperature calculated at 1.21 second at steel side is 586.19°C.

In LAFSW simulation, laser heat input was given to the laser heat affected elements as observed from the cross section from the experiment. The maximum temperature measured at 0.71 second is 949.85°C and 427°C respectively. With passage of time, LAFSW shows almost similar way of heat distribution pattern with increase in maximum temperature compared to FSW simulation. The temperature calculated at 1.21 second is 879.48°C at laser affected area at steel side and 425°C at Al6061 side, but at the same time the temperature at tool bottom at Al6061 side is 497.25°C. Also, at 1.21 second the temperature is found more near the weld zone than at laser affect region at shoulder bottom at steel side. From this it can be predicted that the cooling takes place towards weld zone from outer area at steel side shoulder bottom.

For the heat conduction analysis results of FSW and LAFSW, following conclusion were made:

- The cooling time of Al6061 is higher than SS400 for FSW and LAFSW because of high heat conductivity of Al6061.
- The cooling rate is lower at tool bottom than at shoulder bottom and

tool surface because of the difference in heat affected area in both welding process.

- At steel side in LAFSW, the maximum temperature is found at laser affected area during the commencement of welding and temperature is found decreasing from frictional surface towards base metal at shoulder bottom side.
- The difference in temperature as time passes at a point in FSW is more than that in LAFSW at shoulder bottom. From this it is understood that the heat is conducted more to Al6061 by additional laser preheating, and thus the cooling takes place slowly in LAFSW .

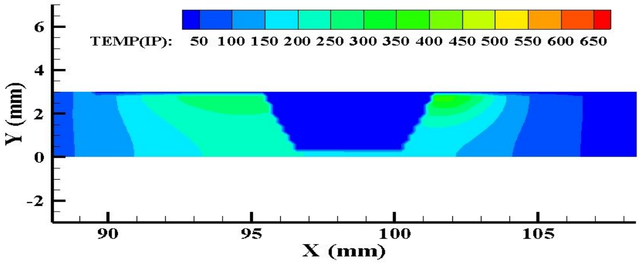

(a) Transient temperature distribution after 0.05 sec.

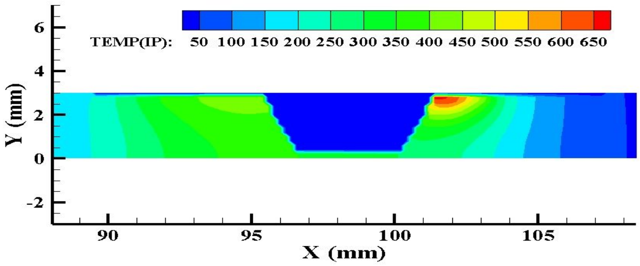

(b) Transient temperature distribution after 0.71 sec.

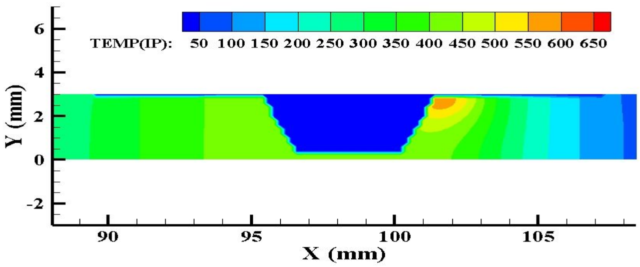

(c) Transient temperature distribution after 1.21 sec.

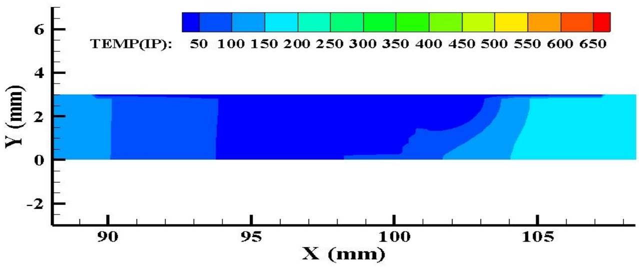

(d) Transient temperature distribution after 6.42 sec.

Fig. 3.5 Heat distribution contour in the model by FSW

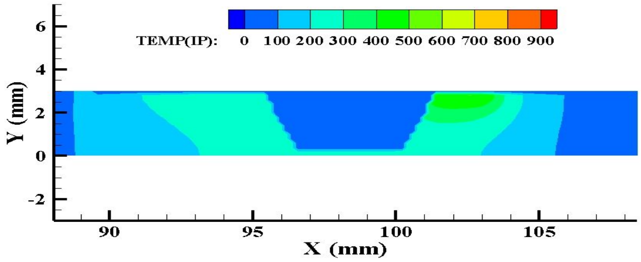

(a) Transient temperature distribution after 0.05 sec.

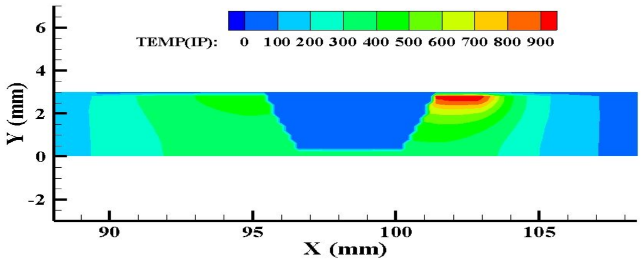

(b) Transient temperature distribution after 0.71 sec.

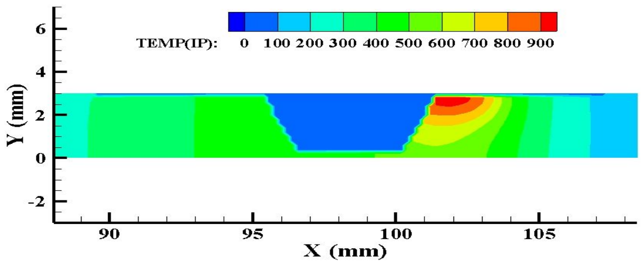

(c) Transient temperature distribution after 1.21 sec.

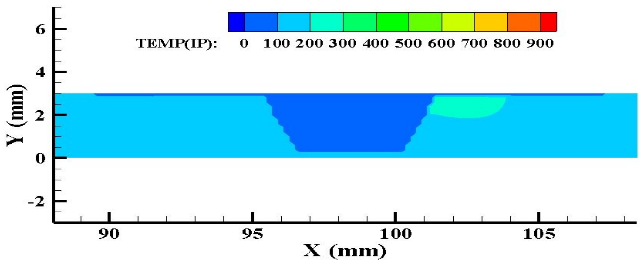

(d) Transient temperature distribution after 8.39 sec.

Fig. 3.6 Heat distribution contour in the model by laser assisted FSW

The thermal characteristics with respect to time for Al6061-T6 and SS400 are shown in Fig.3.7 and 3.8 respectively. Thermal history at 1.4mm below top surface is measured from joint line to distances at 5.5, 8.5, 10.5, 12.5mm towards weld zone at Al6061-T6 side and 1.8, 3 and 5mm towards weld zone at SS400 side. The cooling time is calculated as 3.948 seconds and 8.39 seconds for Al-6061-T6 and SS400 respectively. After this time the temperature decreases gradually to base metal temperature.

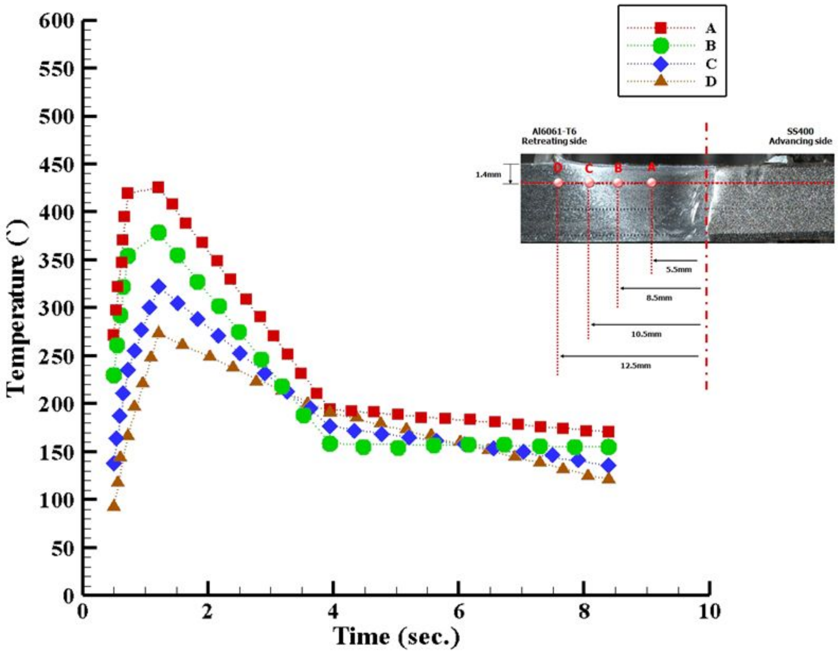

Fig. 3.7 Temperature history of laser assisted FSW -Aluminum side

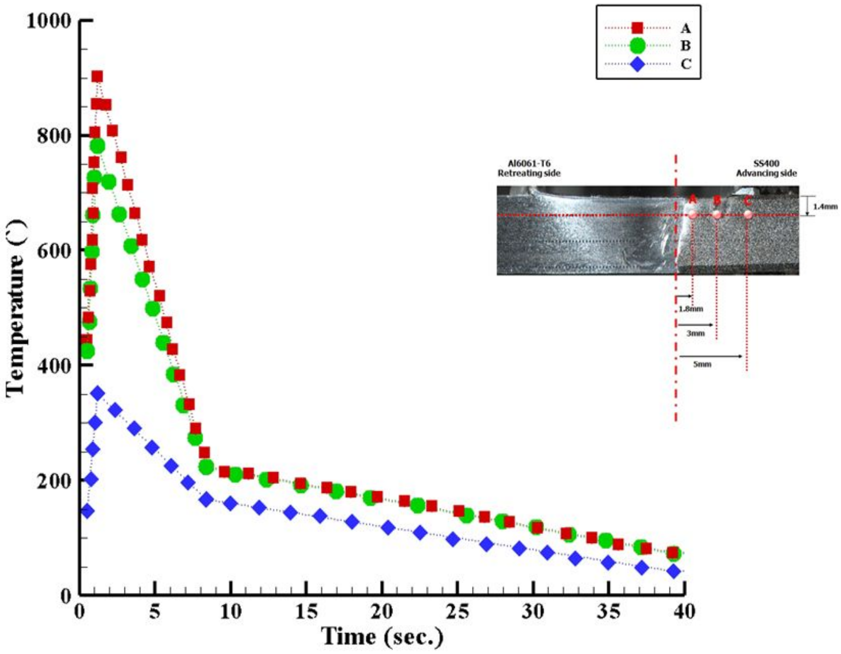

Fig. 3.8 Temperature history of laser assisted FSW
—Steel side

Chapter 4

Experiment of Laser assisted Friction Stir Welding

4.1 Experimental work for laser assisted FSW

4.1.1 Laser-FSW equipment and experimental setup

To conduct laser assisted friction stir welding experiment, WINXEN FSW gantry type system together with MIYACHI Nd:YAG Laser(600W) welding machine was used. FSW Tool system combined with Laser output unit was arranged in order to conduct the welding experiment in X, Y and Z directions. Heat treated STD 11 plate was replaced with mild steel backing plate in order to prevent the backing plate wear.

Fig. 4.1 shows the specification of Nd:YAG Laser and FSW equipment. Laser output unit for preheating the steel material was attached adjacent to the FSW tool shoulder, inclined at 45degrees. The laser spot position of Nd:YAG is placed at a distance of about 10mm from the FSW tool shoulder. When the laser spot is placed near to the tool shoulder, ie, less than 10mm, the thermal plasma affects and damage the tool and therefore the desired preheating is not achieved.

Fig. 4.2 shows the experimental setup for Nd:YAG laser assisted FSW process.

ITEMS		RANGE
TYPE		GANTRY TYPE
Welding Speed	X-axis	0.5~10 mm/sec
	Y-axis	0.5~10 mm/sec
	Z-axis	0.5~10 mm/sec
	R-axis	1~20 RPM
Rotation		300~3000 RPM
LOAD Capacity		Max. 3000Kgf

(a) Equipment and specifications of FSW system

ITEMS	RANGE
Maximum rate output	600 W
Maximum laser energy	100 J/P (10ms pulse width)
Pulse width	Standard: 0.3~100ms (0.1ms increment) Fine setting: 0.25~5ms (0.05ms increment)
Number of output per second	1 to 500 pps
Oscillation wavelength	1.064 ㎛

(b) Equipment and specifications of Nd:YAG Laser system

Fig. 4.1 Specifications of equipment

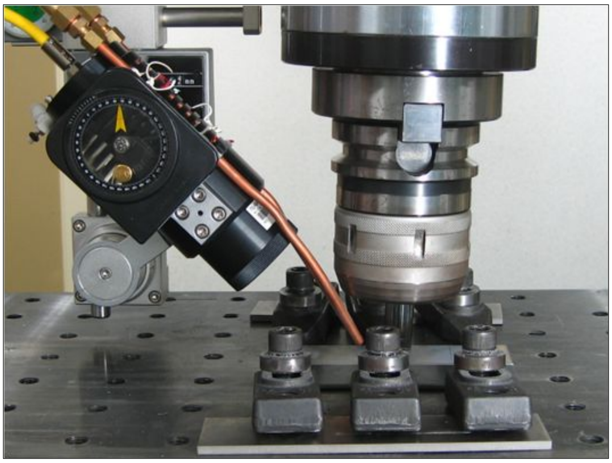

Fig. 4.2 Experimental set-up for laser assisted FSW joint

4.1.2 Description of tool material

The tool material is made of 12%Co tungsten carbide (WF20) to prevent the tool wear due to frictional contact with steel plate while conducting FSW process.

Tool pin shape is of smooth frustum type and shoulder is designed to obtain the proper mixing at the stir zone with good plastic flow of the material. The shoulder is made concave with 3° clearance to act as an escape volume for the material displaced by the probe during the plunge action. The dimensions of shoulder and probe and tool shape to obtain substantial improvements in productivity and quality is shown in Fig 4.3. Table 4.1 shows the Chemical composition and mechanical properties of tungsten carbide tool.

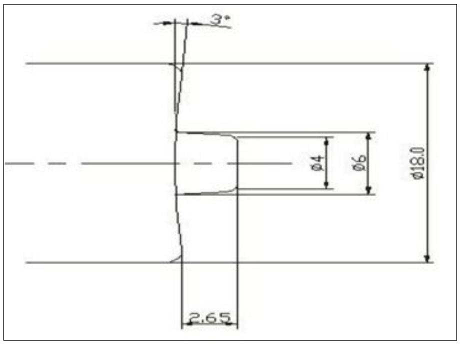

Fig. 4.3 Dimensions and shape of tool

Table. 4.1 Chemical composition and mechanical properties of tool

Grade	WC (±0.5%)	Co (±0.5%)	립도 (㎛)	Density (g/㎤)	Hardness (HRA)	항절력 (Kgf/㎟)	Microstructure
WF20	88	12	0.7	14.08	91.3	370	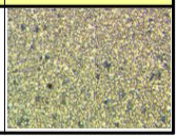

4.2 Experimental work for laser assisted FSW

In the experimental work for LAFSW, laser leading FSW process was carried out where the laser beam was focused 45° to the surface of the weld specimen. Laser focus depth was adjusted to penetrate 1mm on the specimen. Welding parameters such as laser power, pulse width, focal length, number of pulse per second, tool rotating direction, FSW tool−laser distance and tilt angle were kept fixed whereas FSW tool rotating speed, welding speed, laser spot position and shielding gas flow rate were varied.

From the previous researches on FSW of dissimilar materials, it is relevant that join dissimilar plates with tool position at the welding center line is impossible. The difference in hardness and mechanical properties of the materials causes tool wear due to frictional heat at harder material and therefore tool plunge position is adjusted accordingly to conduct LAFSW experiment. The plunge position was kept such that the probe outer face is at a distance 1−1.5mm away from the weld centre line to SS400 side and remaining part of the tool plunges at Al6061−T6 side.

The actual welding process was carried out with tool rotating direction clock wise (cw) placing SS400 in the advancing side and Al6061−T6 in the retreating side. The laser spot was placed at 3mm away from weld center line to SS400 side and 10mm ahead from the shoulder face. Fig. 4.4 shows the schematic of LAFSW process and the welding parameters used. Fig. 4.5 shows the schematic of laser position and tool position.

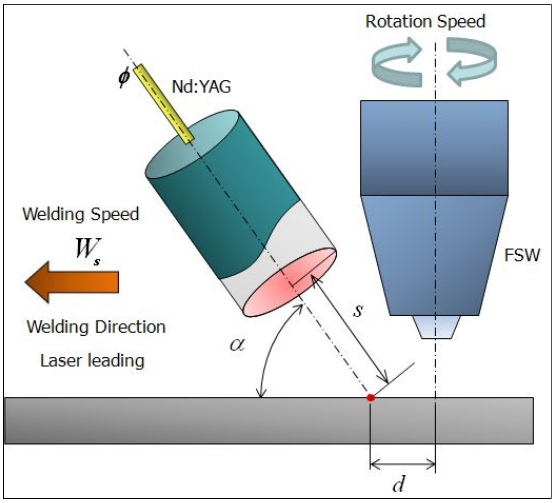

Welding condition		Values
Nd:YAG Pulse Laser	Laser power	460 W
	Pulse width	1 ms
	Lens focal length	Below 1mm on surface
	Laser position	3 ~ 1 mm (at SS400)
	Insert angle of laser	45°
	Oscillation wave length	1.064 μm
	Number of outputs per second	230 pps
FSW	Rotation speed	300 ~ 600 rpm
	Welding speed	0.8~2.4 mm/s (per 0.2)
	Insert depth of pin	2.65 ~ 2.75
	Tilt angle	2°
Laser-FSW Distance = 10 (mm)		
Pin position (Al6061-T6 : SS400) = 9 : 1		
Direction of rotation = CW		
Leading condition = Laser leading		
Shield gas flow = 0, 4, 20 l/min		
Room temperature = 20°		

Fig. 4.4 Schematic diagram and welding parameters of LAFSW

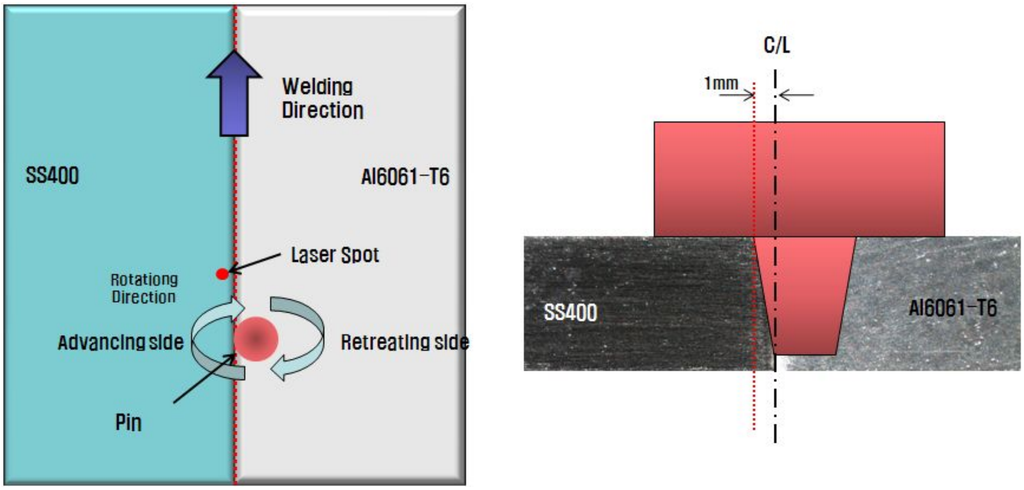

Fig. 4.5 Schematic of laser and tool position

4.2.1 Experiment to obtain optimum laser preheating

Experiment to obtain optimum laser preheating was carried out on SS400 plate and the results are given in Table.4.2. From the bead shapes obtained and macro image observation, laser output power of 406W found optimum to give preheating on SS400 plate. At this laser power, a penetration depth of 0.8mm and bead with of 1.6mm was obtained. Later this laser preheating parameters was found accurate to obtain sound dissimilar weld joint by LAFSW.

Table. 4.2 Conditions for laser preheating

No.	Material		Welding Condition					
			Reference value (J)	Number of outputs per second (PPS)	Laser power (W)	Welding speed (mm/s)	Insert angle (°)	Shield gas Flow (ℓ/min)
1	SS400		3	110	327	1.0	45	-
	Bead shape and Macro images	Top						
		Back						
2	SS400		2	230	406	1.0	45	-
	Bead shape and Macro images	Top						
		Back						
3	SS400		2.5	200	446	1.0	45	-
	Bead shape and Macro images	Top	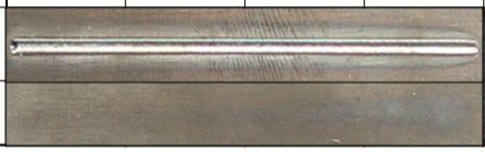					
		Back						

4.2.2 Experiment by FSW

From many trials of experiment carried out on dissimilar joint by FSW, best 16 trials was considered and the welding conditions are tabulated as given in Table 4.3. The bead shapes of the best 16 trials are shown in Table 4.4. Rotation speed of the tool, tool travel speed and tool rotating direction were varied to obtain better results. Initial trials were done for obtaining better surface beads with proper exit holes. At 500~600rpm and at various welding speeds, from the macro images, it was observed that the presence of mild steel deposits are more in the aluminium stir zone which can seriously affect the mechanical characteristics of weld joint. From the FSW experiments and macro images, tool rotation at 400rpm and at tool travel speed 0.8~1.2mm/sec was found good. At a tool speed of 300rpm and 0.6mm/sec, porosity is appeared in Al6061-T6 as observed from the macro image. At 500rpm the weld defects were found due to more heat generation at tool work piece interface.

At 400rpm and 1.2mm/sec welding speed, good bead shape is obtianed and onion ring structure is clearly visible.

Table 4.3 FSW parameters

No.	Material	Adv. side	Tool plunge point	Rotating Speed (rpm)	Travel Speed (mm/s)	Rotation Direction
1	Al−SS400	SS400	9:1	300	0.6	cw
2	Al−SS400	SS400	9:1	300	0.8	cw
3	Al−SS400	SS400	9:1	300	1.0	cw
4	Al−SS400	SS400	9:1	300	1.2	cw
5	Al−SS400	SS400	9:1	400	0.6	cw
6	Al−SS400	SS400	9:1	400	0.8	cw
7	Al−SS400	SS400	9:1	400	1.0	cw
8	Al−SS400	SS400	9:1	400	1.2	cw
9	Al−SS400	SS400	9:1	500	0.6	cw
10	Al−SS400	SS400	9:1	500	0.8	cw
11	Al−SS400	SS400	9:1	500	1.0	cw
12	Al−SS400	SS400	9:1	500	1.2	cw
13	Al−SS400	SS400	9:1	600	0.6	cw
14	Al−SS400	SS400	9:1	600	0.8	cw
15	Al−SS400	SS400	9:1	600	1.0	cw
16	Al−SS400	SS400	9:1	600	1.2	cw

Table 4.4 Bead shapes of FSW weldment

RPM	Travel speed (mm/s)	Bead shape	Macro image
300	0.6		
	0.8		
	1.0		
	1.2		
400	0.6		
	0.8		
	1.0		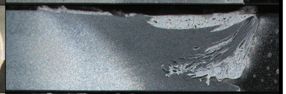
	1.2		
500	0.6		
	0.8		
	1.0		
	1.2		
600	0.6		–
	0.8		–
	1.0		–
	1.2		–

4.2.3 Experiment by laser assisted FSW(LAFSW)

Welding conditions of 30 experiment trials are tabulated in Table 4.5. Table 4.6 shows bead shapes for dissimilar joint of Al6061-T6 and SS400 butt joint. For Laser-FSW process, the best welding parameters obtained from the FSW experiments and laser preheating BOP test conditions were considered respectively. At all tool rotation speed, the back bead was very clearly obtained in LAFSW compared to FSW. Good welding conditions are obtained at tool rotation speeds 300 and 400rpm at 1.6, 2.0 and 1.4, 2.0mm/sec welding speed respectively from the bead shape and macro image observations. At same welding speed of 0.8 and 1.0mm/sec poor bead is obtained at 400rpm compared to 300rpm tool rotation speed. Higher welding speed at 400rpm leads to poor weld formation due to low heat input and low friction stirring. Poor weld joints were obtained at 500~600rpm due to high heat generation at tool- workpiece interface.

Table 4.5 LAFSW parameters

No.	Material	Tool plunge point	Rotating Speed	Travel Speed	Rotation Direction	Laser Power (W)	Laser Length (ms)	Shield Gas (l/min)	Torch Angle
1	Al-SS400	9:1	300	0.8	cw	460/ 405.3	1	4	45
2	Al-SS400	9:1	300	1.0	cw	460/ 406.3	1	4	45
3	Al-SS400	9:1	300	1.2	cw	460/ 406.6	1	4	45
4	Al-SS400	9:1	300	1.4	cw	460/ 406.9	1	4	45
5	Al-SS400	9:1	300	1.6	cw	460/ 407.1	1	4	45
6	Al-SS400	9:1	300	1.8	cw	460/ 407	1	4	45
7	Al-SS400	9:1	300	2.0	cw	460/ 407.1	1	4	45
8	Al-SS400	9:1	400	0.8	cw	460/ 405.6	1	4	45
9	Al-SS400	9:1	400	1.0	cw	460/ 406.7	1	4	45
10	Al-SS400	9:1	400	1.2	cw	460/ 406.4	1	4	45
11	Al-SS400	9:1	400	1.4	cw	460/ 406.6	1	4	45

No.	Material	Tool plunge point	Rotating Speed	Travel Speed	Rotation Direction	Laser Power (W)	Laser Length (ms)	Shield Gas (l/min)	Torch Angle
12	Al-SS400	9:1	400	1.6	cw	460/ 406.1	1	4	45
13	Al-SS400	9:1	400	1.8	cw	460/ 405.7	1	4	45
14	Al-SS400	9:1	400	2.0	cw	460/ 406	1	4	45
15	Al-SS400	9:1	400	2.2	cw	460/ 406.3	1	4	45
16	Al-SS400	9:1	400	2.4	cw	460/ 406.7	1	4	45
17	Al-SS400	9:1	500	1.2.	cw	460/ 405.1	1	4	45
18	Al-SS400	9:1	500	1.4	cw	460/ 406	1	4	45
19	Al-SS400	9:1	500	1.6	cw	460/ 406.2	1	4	45
20	Al-SS400	9:1	500	1.8	cw	460/ 406.3	1	4	45
21	Al-SS400	9:1	500	2.0	cw	460/ 406.1	1	4	45
22	Al-SS400	9:1	500	2.2	cw	460/ 406.3	1	4	45
23	Al-SS400	9:1	500	2.4	cw	460/ 406.	1	4	45
24	Al-SS400	9:1	600	1.2	cw	460/ 405.3	1	4	45
25	Al-SS400	9:1	500	1.4	cw	460/ 405.2	1	4	45
26	Al-SS400	9:1	500	1.6	cw	460/ 404.6	1	4	45

No.	Material	Tool plunge point	Rotating Speed	Travel Speed	Rotation Direction	Laser Power (W)	Laser Length (ms)	Shield Gas (l/min)	Torch Angle
27	Al-SS400	9:1	500	1.8	cw	460/ 406.3	1	4	45
28	Al-SS400	9:1	500	2.0	cw	460/ 405.8	1	4	45
29	Al-SS400	9:1	500	2.2	cw	460/ 406.2	1	4	45
30	Al-SS400	9:1	500	2.4	cw	460/ 406.2	1	4	45

Table 4.6 Bead shapes of LAFSW weldment

RPM	Travel speed (mm/s)	Laser power : 460W / lens focal length: −1mm on surface insert angle : 45°/ shield gas : 4 l/min		
		Bead shape		Macro image
300	0.8	Top		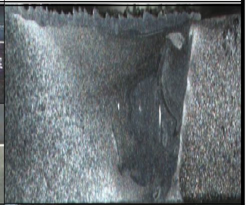
		Bottom		
	1.0	Top		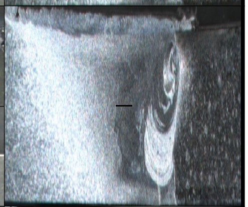
		Bottom		
	1.2	Top		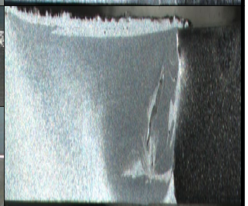
		Bottom		
	1.4	Top		
		Bottom		
	1.6	Top		
		Bottom		
	1.8	Top		
		Bottom		
	2.0	Top		
		Bottom		

RPM	Travel speed (mm/s)	Laser power : 460W / lens focal length: −1mm on surface insert angle : 45°/ shield gas : 4 l/min		
		Bead shape		Macro image
400	0.8	Top		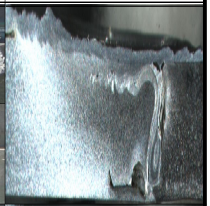
		Bottom		
	1.0	Top		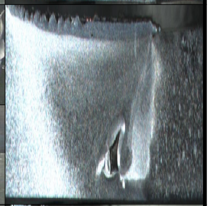
		Bottom	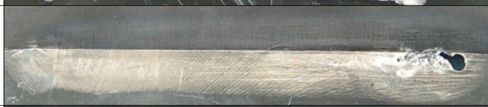	
	1.2	Top	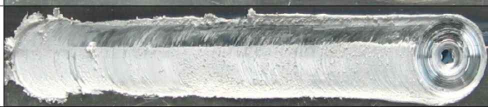	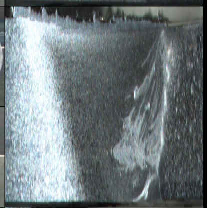
		Bottom		
	1.4	Top		
		Bottom		
	1.6	Top	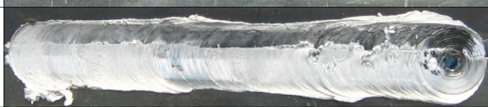	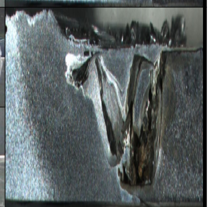
		Bottom		
	1.8	Top	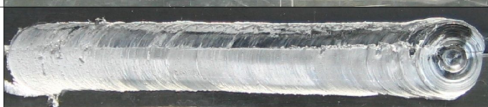	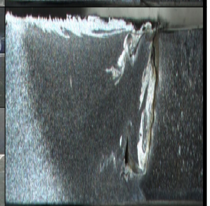
		Bottom		
	2.0	Top		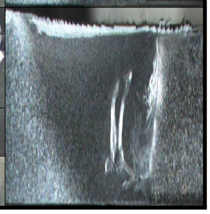
		Bottom		

RPM	Travel speed (mm/s)	Laser power : 460W / lens focal length: −1mm on surface insert angle : 45°/ shield gas : 4 l/min		
			Bead shape	Macro image
400	2.2	Top	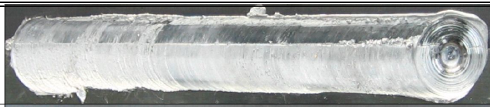	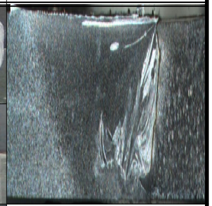
		Bottom		
	2.4	Top		−
		Bottom		
500	1.2	Top		−
		Bottom		
	1.4	Top		−
		Bottom		
	1.6	Top		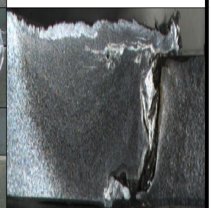
		Bottom		
	1.8	Top		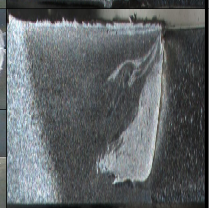
		Bottom		
	2.0	Top		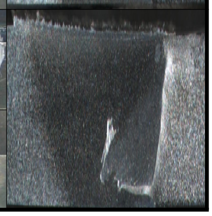
		Bottom		

RPM	Travel speed (mm/s)	Laser power : 460W / lens focal length: −1mm on surface insert angle : 45°/ shield gas : 4 l/min		
		Bead shape		Macro image
500	2.2	Top		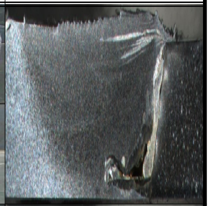
		Bottom		
	2.4	Top	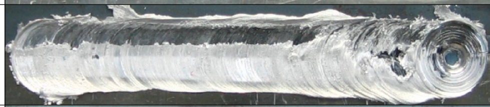	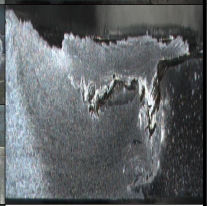
		Bottom		
600	1.2	Top		–
		Bottom		
	1.4	Top		–
		Bottom		
	1.6	Top	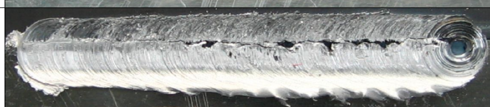	–
		Bottom		
	1.8	Top		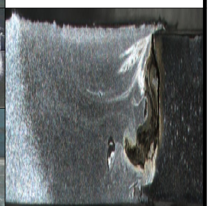
		Bottom		
	2.0	Top		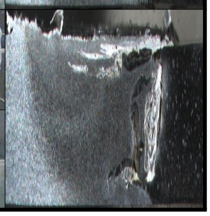
		Bottom		

<table>
<tr><th rowspan="2">RPM</th><th rowspan="2">Travel speed (mm/s)</th><th colspan="3">Laser power : 460W / lens focal length: −1mm on surface
insert angle : 45°/ shield gas : 4 l/min</th></tr>
<tr><th colspan="2">Bead shape</th><th>Macro image</th></tr>
<tr><td rowspan="4">600</td><td rowspan="2">2.2</td><td>Top</td><td></td><td rowspan="2">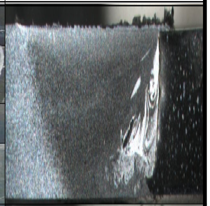</td></tr>
<tr><td>Bottom</td><td></td></tr>
<tr><td rowspan="2">2.4</td><td>Top</td><td></td><td rowspan="2"></td></tr>
<tr><td>Bottom</td><td>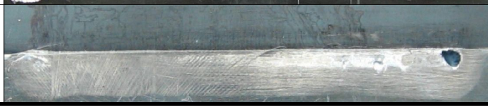</td></tr>
</table>

4.3 Tensile test results

4.3.1 Tensile test

Tensile test specimens are cut perpendicular to the weld length (Fig4.6) to carry out the tensile test experiment of dissimilar joint by LAFSW. The specimen dimensions are given in Table.4.7. Tensile test was done with Load speed 0.033mm/sec and Stress-Strain curve was obtained.

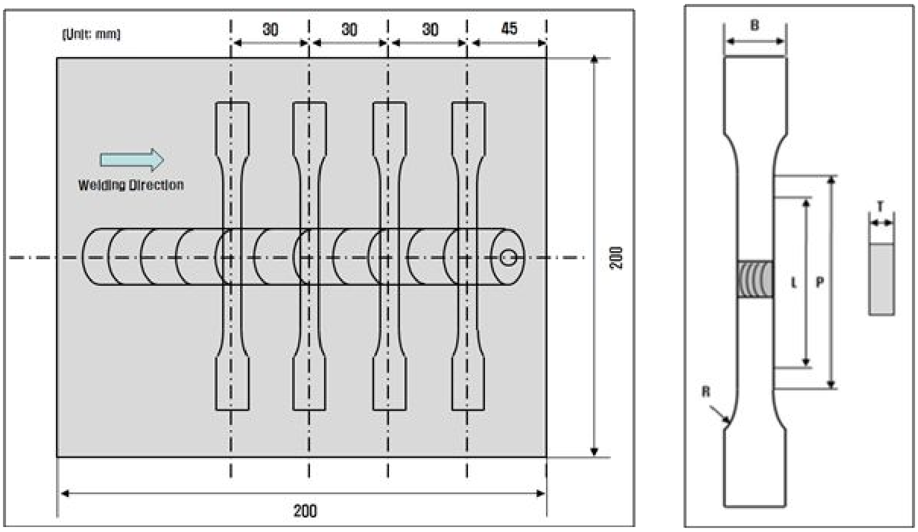

Fig. 4.6 Tensile test specimen details

Table 4.7 Tensile test specimen dimensions

Specimen STD. (KS B 0801 13B)	Dimension (mm)					
	W	L	P	R	T	B
	12.5	50	60	20	3	20
Load Speed (mm/s)	0.033					

4.3.2 Tensile test for similar joint (Al6061-T6)

Tensile test of similar joint of Al6061-T6 was carried out to understand the tensile strength of FSW joint made at 500rpm and 1.6mm/sec tool travel speed (Table 4.8). Testing was carried out as per korean standards. This result The tensile strength of the FSW weld joint was obtained as 256.4MPa which is 77% of the tensile strength of base metal (330MPa).

Table 4.8 Tensile tested similar joint

<table>
<tr><th>Rotation Speed (rpm)</th><th>Travel speed (mm/s)</th><th colspan="2">Bead shape</th></tr>
<tr><td rowspan="5">500</td><td rowspan="5">1.6</td><td>Top</td><td></td></tr>
<tr><td>Bottom</td><td></td></tr>
<tr><td colspan="2">Tensile tested specimen</td></tr>
<tr><td>
</td><td>256.4 MPa
(330)</td></tr>
<tr><td colspan="2">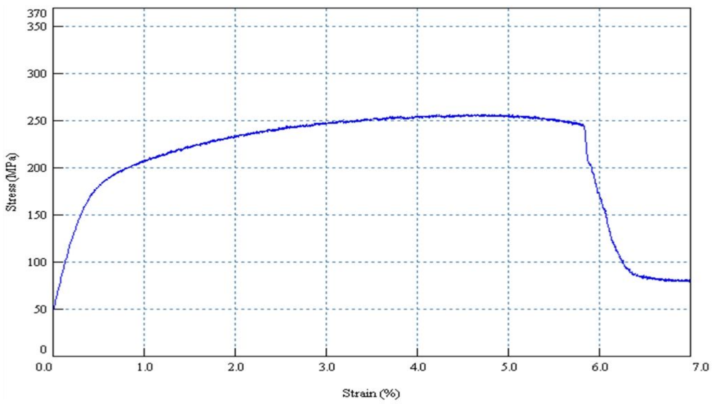
</td></tr>
</table>

4.3.3 Tensile test of FSW dissimilar joint

Testing of tensile strength of dissimilar weld joint by FSW was carried out as per korean standards. The tensile test results (Table 4.9) reveals that fracture occurs at the dissimilar joint interface. The fracture was occurred at the weld joint interface and maximum tensile strength was 315.6MPa, which is 95% of the aluminum alloy base metal tensile strength(330MPa).

From stress−strain curve it is evident that the specimen is subjected to brittle fracture(Table 4.10). Good tensile strength is obtained for the weld joint made at tool rotation 400RPM and travel speed 1.2mm/s.

Table 4.9 Fractured specimens and cross sections of dissimilar joint by FSW

RPM	Travel speed (mm/s)	Fractured specimens	Macro image	T.S (MPa)
300	0.6	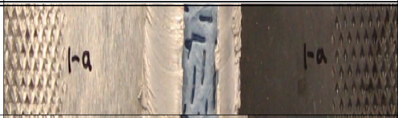	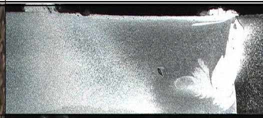	173.1
	0.8		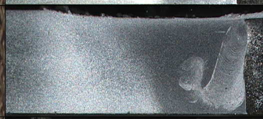	108.9
	1.0		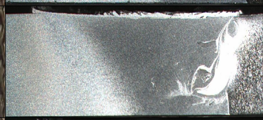	243.6
	1.2			235.6
400	0.6	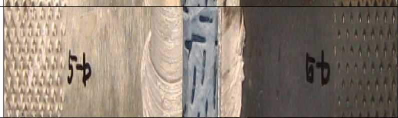		265.3
	0.8	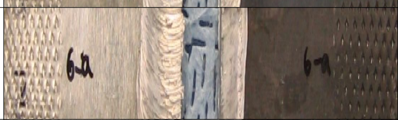		310
	1.0			308.9
	1.2			315.6
500	0.6	–		교반불량
	0.8	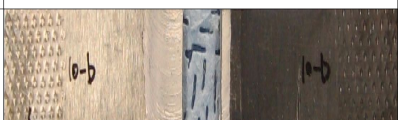		152.8
	1.0	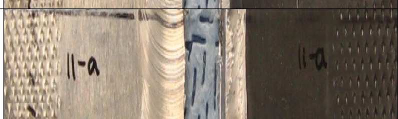		201.4
	1.2			301.1

Table 4.10 Stress−strain curve for dissimilar weld joint by FSW

RPM	Travel speed(mm/s)			
	0.6	0.8	1.0	1.2
300	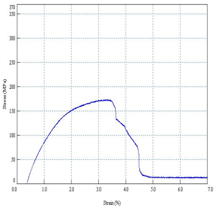	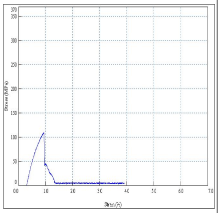	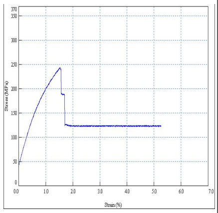	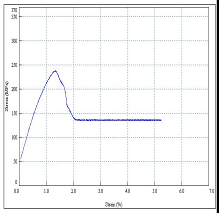
400	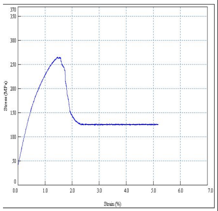	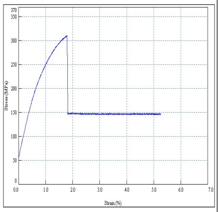	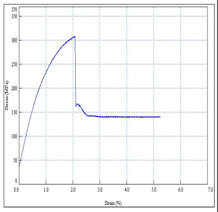	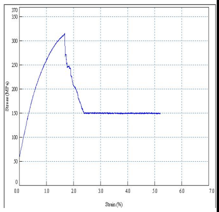
500	−	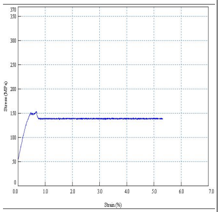	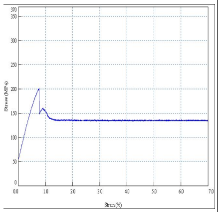	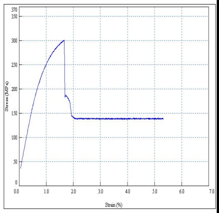

4.3.4 Tensile test of laser assisted FSW dissimilar joint

The weld cross sections and fractured specimens by tensile test of dissimilar joint by Laser assisted FSW shown in Table 4.11. As observed from the tensile test results, the fracture occurred at the joint interface in specimens welded at 300~500rpm tool rotation speed. The tensile strength of dissimilar joint by LAFSW was found 80~95% than that of Al6061-T6 base metal. From the stress strain curve (Table 4.12), at 400rpm and 1.4mm/sec the tensile strength of Aluminum was 340MPa which is above base metal tensile strength (330MPa). Weld specimens at 400rpm and 1.4mm/sec failed in a ductile like fracture mode where as the specimen fractured in a brittle way for 400rpm and 2.0mm/sec.

Table 4.11 Fractured specimens and cross sections of dissimilar joint by laser assisted FSW

RPM	Travel speed (mm/s)	Fractured specimens	Macro image	T.S (MPa)
300	0.8	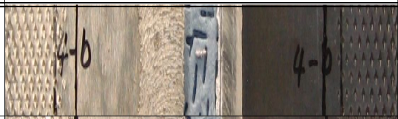		101.9
	1.0			251.7
	1.2			281.9
	1.4	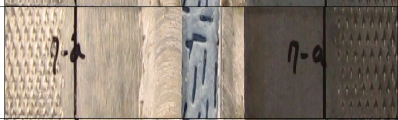	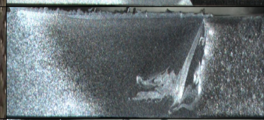	283.1
	1.6	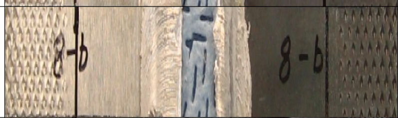		333.3
	1.8			234.2
	2.0			315.3
400	0.8			259.2
	1.0			251.7
	1.2			260.0
	1.4	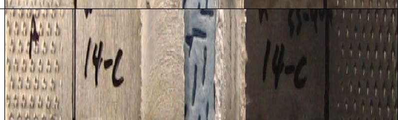		340.0
	1.6	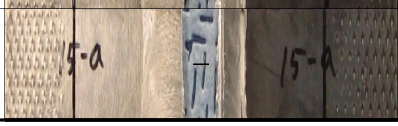	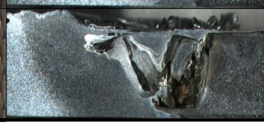	258.1

RPM	Travel speed (mm/s)	Fractured specimens	Macro image	T.S (MPa)
400	1.8		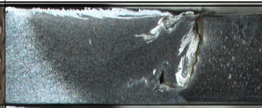	150.8
	2.0			299.7
	2.2			151.1
500	1.6			154.2
	1.8			245.3
	2.0	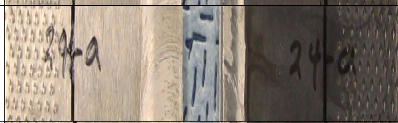		280.8
	2.2		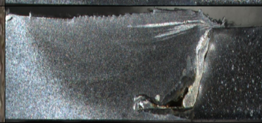	183.1
	2.4		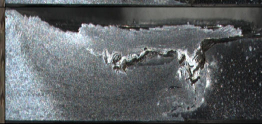	179.7
600	1.8	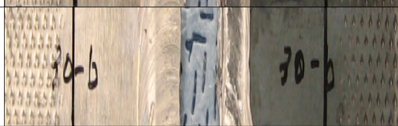		153.1
	2.0	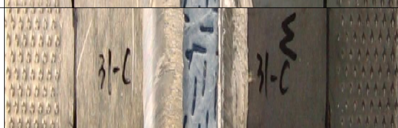		252.2
	2.2	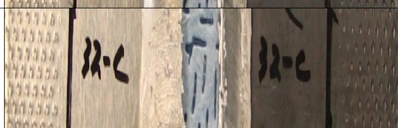		180.8
	2.4	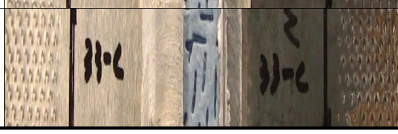		247.5

Table 4.12 Stress-strain curve of dissimilar weld joint by LAFSW

RPM	Travel speed(mm/s)		
	1.0	1.2	1.4
300	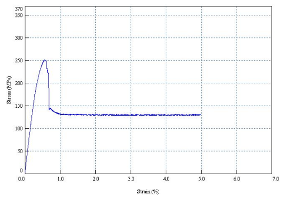	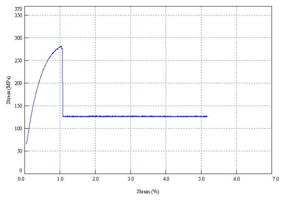	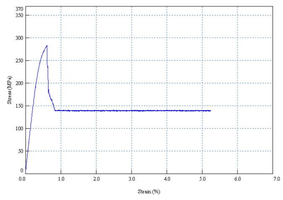
	1.6	1.8	2.0
	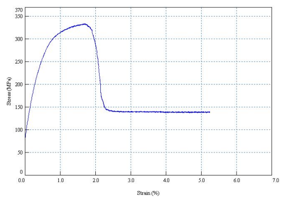	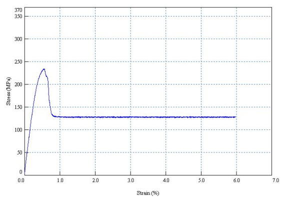	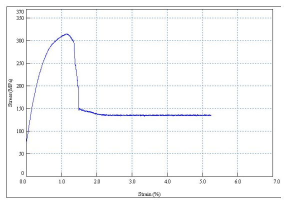
	0.8	1.0	1.2
	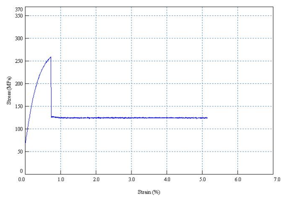	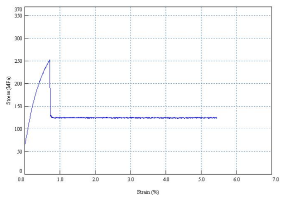	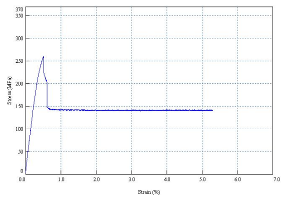
400	1.4	1.6	1.8
	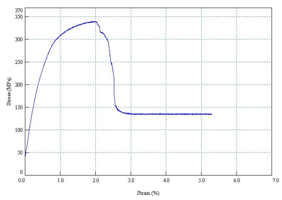	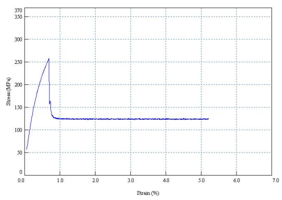	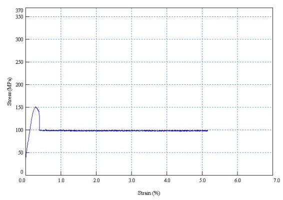
	2.0	2.2	-
	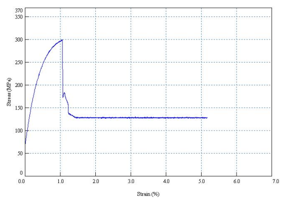	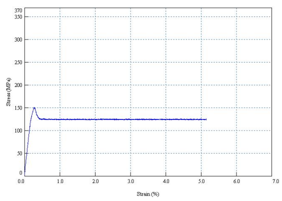	

<table>
<tr><th rowspan="2">RPM</th><th colspan="3">Travel speed(mm/s)</th></tr>
<tr><th>1.6</th><th>1.8</th><th>2.0</th></tr>
<tr><td rowspan="4">500</td><td>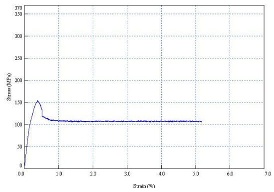</td><td>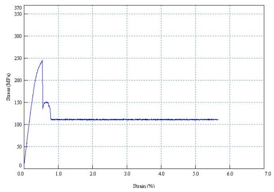</td><td>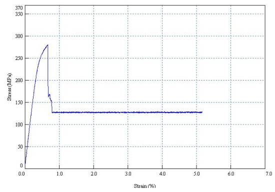</td></tr>
<tr><td>2.2</td><td>2.4</td><td>–</td></tr>
<tr><td>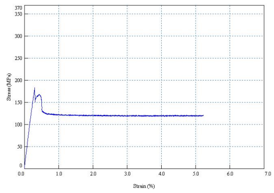</td><td>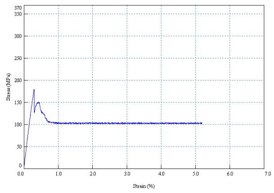</td><td>–</td></tr>
<tr><td>1.8</td><td>2.0</td><td>2.2</td></tr>
<tr><td rowspan="3">600</td><td>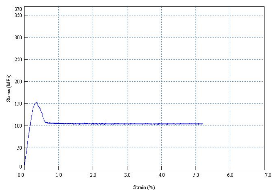</td><td>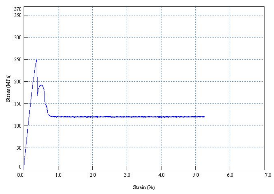</td><td>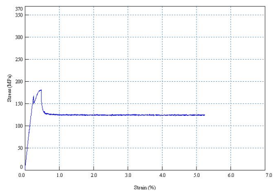</td></tr>
<tr><td>2.4</td><td>–</td><td>–</td></tr>
<tr><td>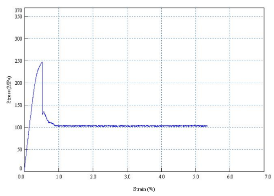</td><td></td><td></td></tr>
</table>

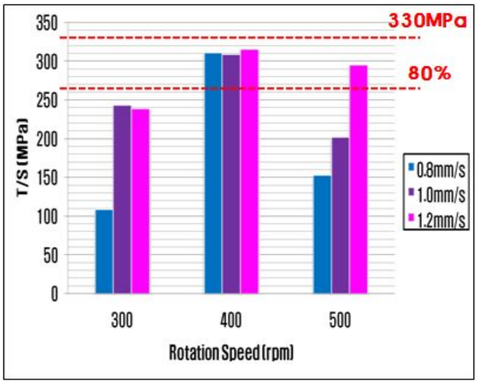

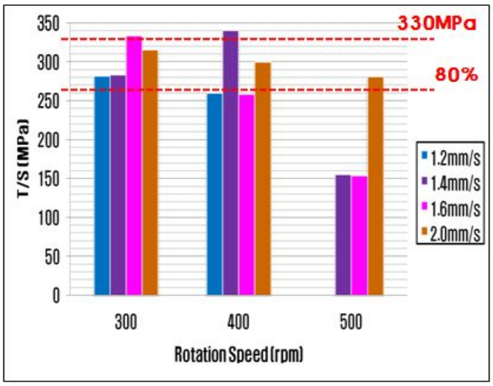

(a) FSW (B) LAFSW

Fig. 4.7 Rotation speed versus tensile strength

Comparing the results of FSW and LAFSW, tensile strength of LAFSW shows better than FSW(Fig.4.7). Tensile strength of above 80% of base metal is obtained only at 300rpm in case of FSW joint whereas LAFSW weld joint made at 300rpm and 400rpm at welding speeds 1.2~2.0mm/sec gives better tensile strength. The tensile strength of LAFSW was 80~95% of base metal and best tensile strength value (340MPa) is obtained at a welding speed of 400rpm and 1.4mm/sec welding speed. Therefore, weld joint with better tensile strength can be made at higher welding speed by LAFSW than by FSW

4.4 Hardness test results

4.4.1 Hardness test

The hardness of a weld specimen was measured using Akashi HM−112 Vickers Hardness tester. The indenter employed in the Vickers test was a square−based pyramid whose opposite sides meet at the apex at an angle of 136° with load 500g applied for 10 sec.

Fig. 4.8 and 4.9 shows the Vickers hardness tester and test specimen respectively. The hardness test was carried out on the welded specimen at 0.25 gap at three different positions at 1mm distance apart.

	values
Type	Micro vickers hardness tester
Load	0.5 Kgf
Loading time	10 sec.
Test position	bellow 0.75, 1.75, 2.75 on surface

Fig. 4.8 Vickers hardness test machine and specimen

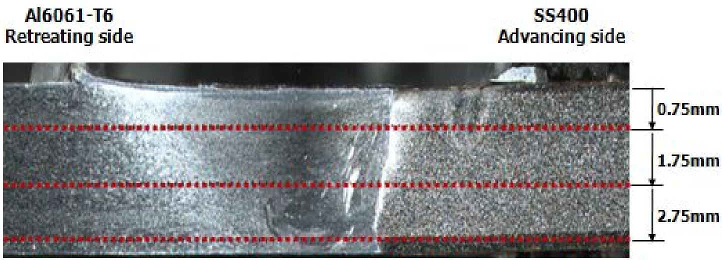

Fig. 4.9 Vickers hardness test machine and specimen

4.4.2 Hardness result

The hardness distributions of dissimilar joint by LAFSW at 400rpm and 1.4mm/sec is shown in Fig.4.10. A drop in hardness from parent metal hardness is evident in the welding zone for Al6061-T6. Precipitation hardening alloys such as the Al6061-T6 show a loss of hardness in the HAZ, with some recovery in the nugget because a lower hardness due to the absence of strengthening precipitates at HAZ and the dissolved precipitates do re-precipitate or recrystallize subsequently at higher temperatures in the nugget zone. The hardness of Al6061-T6 at the TMAZ and SZ is more than HAZ because of the mechanical effect of plastic flow during weld formation.

On SS400, the hardness value at weld zone is more than that of base metal due to work hardening effect by laser preheating and frictional heating. The base metal hardness of Al6061-T6 and SS400 are 97HV and 121HV respectively. The hardness values HAZ, TMAZ and SZ of Al6061-T6 are 62, 73 and 78HV respectively.

The hardness of the weld nugget shows variable values because of the presence of the fine or coarse dispersed stainless steel particles in the weld nugget.

When comparing hardness results (Fig 4.11) of LAFSW with FSW, hardness values are found more in LAFSW. This is because, plastic flow is increased by laser preheating making finer recrystallized grains at the TMAZ and SZ.

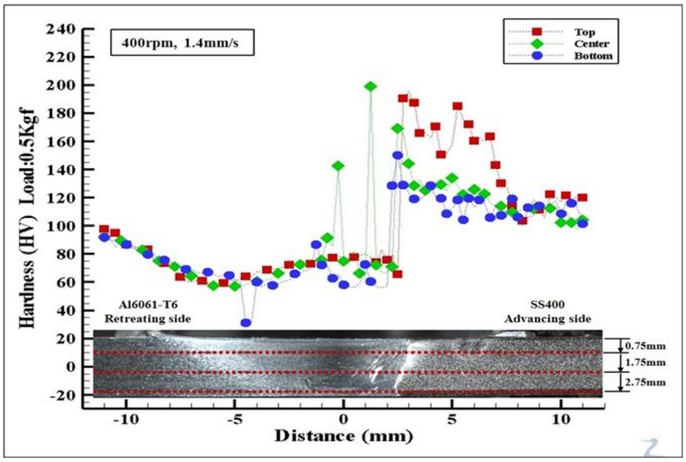

Fig. 4.10 Hardness testing result of LAFSW

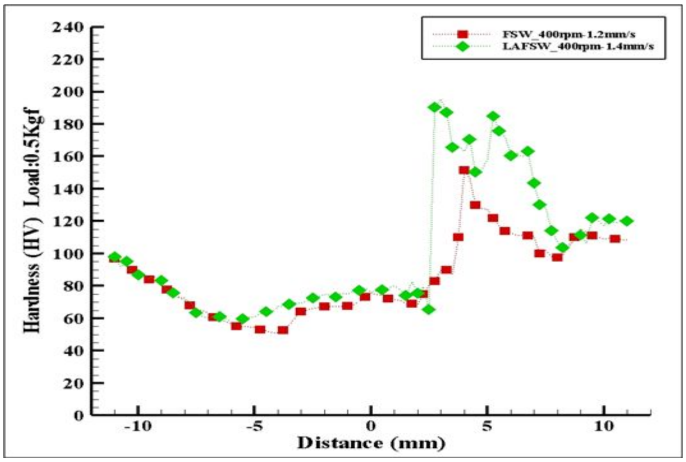

Fig. 4.11 Hardness testing result of FSW and LAFSW

4.5 Microstructure analysis of dissimilar joint

4.5.1 Microstructure analysis

Microstructure analysis of dissimilar joint by LAFSW was carried out with the weld cross-section cut form the welded specimen. The cut specimen is polished and etched using the mixture of 1.5㎖ Nitric acid, 3㎖ Hydro chloric acid, 3㎖ Hydro fluoric acid and 100㎖ distilled water for Al6061-T6 and 3ml Nitric acid with 100ml Ethyl alcohol for SS400. The etching was done for 80sec for Al6061-T6 and 45sec for SS400. The prepared specimen was mounted on OLYMPUS optical microscope to observe the micro structure as shown in Fig. 4.12.

Fig. 4.12 Optical microscope

4.5.2 Microstructure of FSW dissimilar joint

Microstructure of FSW dissimilar joint at different points of weld zone is shown in Fig. 4.13. The base metal (point 'a') and HAZ (point 'b') exhibits almost similar microstructure in Al6061−T6 with grain size little bigger in HAZ than base metal. The TMAZ (point 'c') is characterized by a highly deformed structure. The parent metal elongated grains were deformed in an upward flowing pattern around the nugget zone. Although TMAZ underwent plastic deformation, recrystallization did not occur in this zone due to insufficient deformation strain. However dissolution of some precipitates was observed in the TMAZ. The weld nugget (point 'd') exhibits a mixture of Al alloy and SS400 particles pulled away by forge of tool pin from the stainless steel surface.

Therefore the weld nugget has a composite structure of SS400 particles reinforced Al6061−T6 alloy and have an irregular shape and inhomogeneous distribution within the weld nugget..

microstructure of position		
(a) Base Metal (Al6061−T6)	(b) HAZ (Al6061−T6)	(c) TMAZ (Al6061−T6)
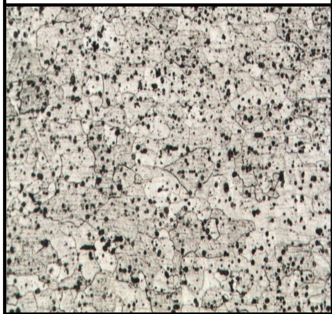	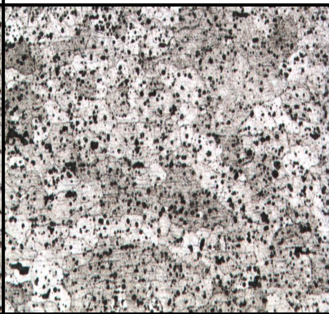	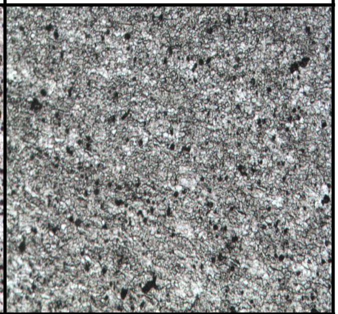
(d) Stir Zone (Al6061−T6)	(e) Bonding Interface (Al6061−T6 and SS400)	(f) Base Metal (SS400)
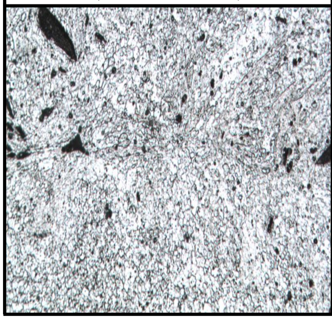	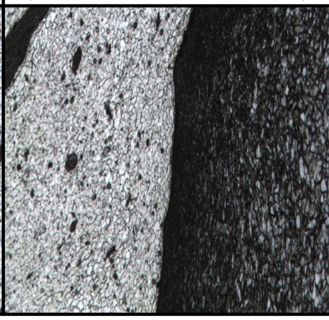	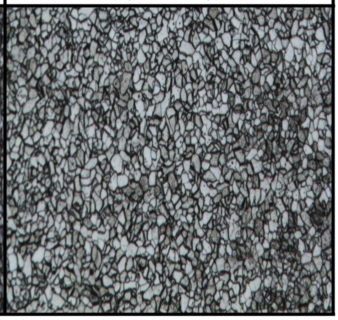

Fig. 4.13 Microstructural (FSW)

4.5.3 Microstructure of laser assisted FSW dissimilar joint

Microstructure of LAFSW dissimilar joint is shown in Fig. 4.14.

The microstructure at HAZ in LAFSW is almost similar to FSW, but the grain size is smaller in TMAZ of Al6061-T6 by LAFSW than in FSW. And in TMAZ, the parent metal elongated grains were deformed in same direction around the nugget zone. At nugget zone, coarse grain size is appeared in LAFSW when compared to FSW because of more plastic flow due to laser preheating effect. A solidified microstructure is first formed by the laser preheating which is the preceeding heat source at SS400 side. The solidification microstructure then disappears by the stir action of the tool and then refined ferrite-bainite microstructure is formed. The bonding interface microstructure is quite similar to that obtained by the normal FSW.

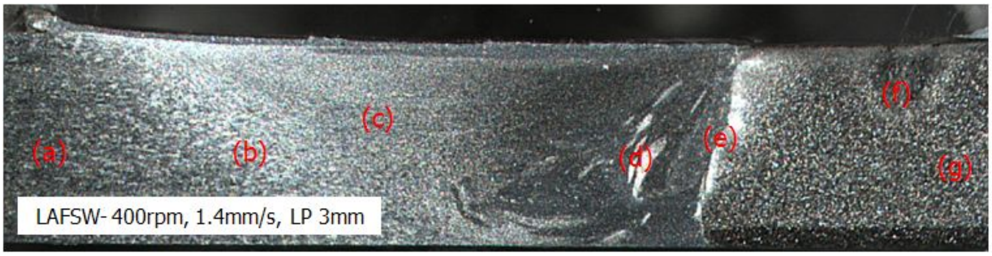

microstructure of position		
(a) Base Metal (Al6061−T6)	(b) HAZ (Al6061−T6)	(c) TMAZ (Al6061−T6)
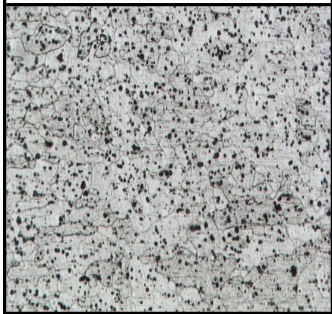		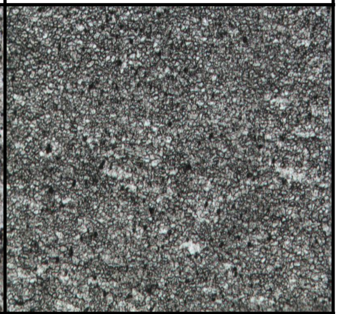
(d) Stir Zone (Al6061−T6)	(e) Bonding Interface (Al6061−T6 and SS400)	(f) Laser Weld Metal (SS400)
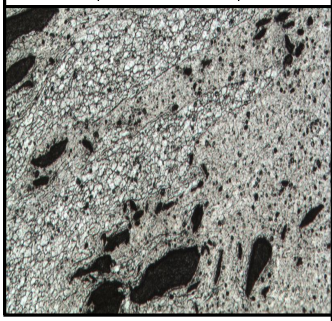	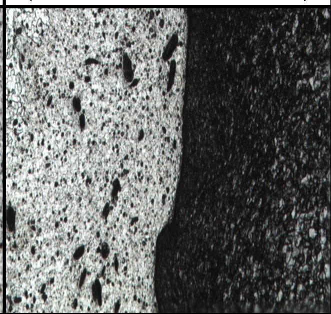	
	(g) Base Metal (SS400)	
	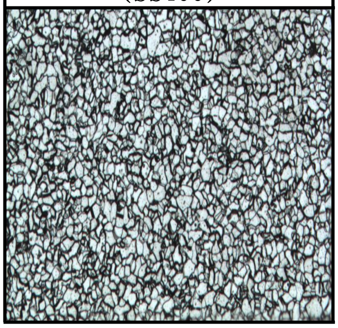	

Fig. 4.14 Microstructural (LAFSW)

4.6 Analysis of weld specimen using SEM and EDS observation

4.6.1 SEM of fractured specimens

The SEM microstructures of the fractured specimens have been illustrated in Fig4.15. The images of top, middle and bottom side of the fractured surface of Al6061 and SS400 were observed for weld joint by FSW. The fracture surface shows a dimple pattern on all check points. But middle and bottom check points is subjected to brittle fracture. At SS400 side, Top check point is subjected to ductile fracture and middle check point is subjected to ductile and brittle fracture, where as at bottom check point, complete brittle fracture is occurred.

From the SEM image observation of as-received dissimilar joint by LAFSW (Fig.4.16), dimple pattern is observed at the fractured surface in Al6061-T6 side associated with ductile fracture. Steel inclusions were found in the middle and bottom part of Al6061-T6 side. At SS400 side, top side shows dimple patterns associated with ductile fracture wherein middle side mixed mode of cleavage area and ductile fracture was observed. At bottom side, is subjected to ductile and brittle fracture.

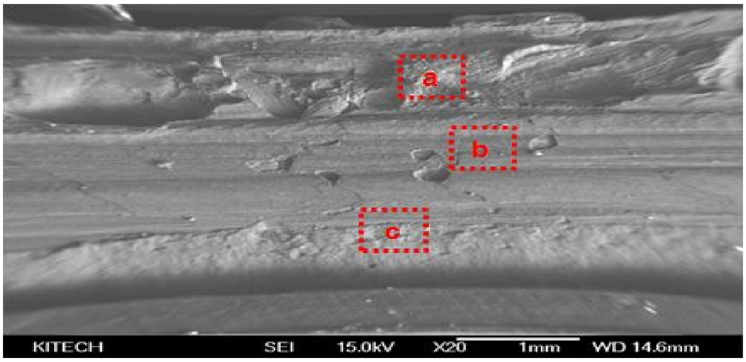

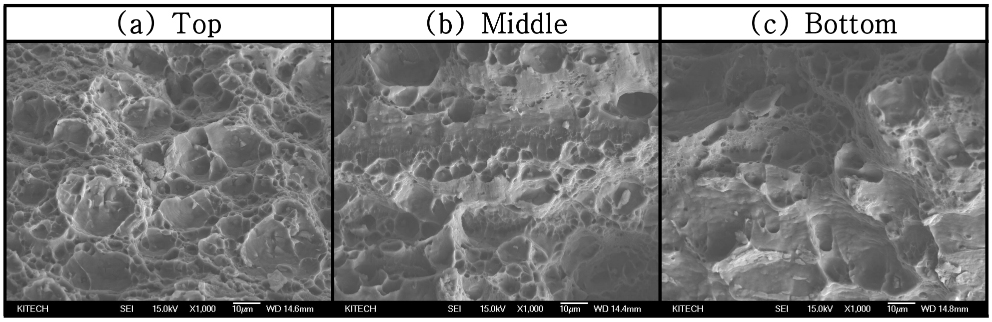

(a)FSW- Al6061 side

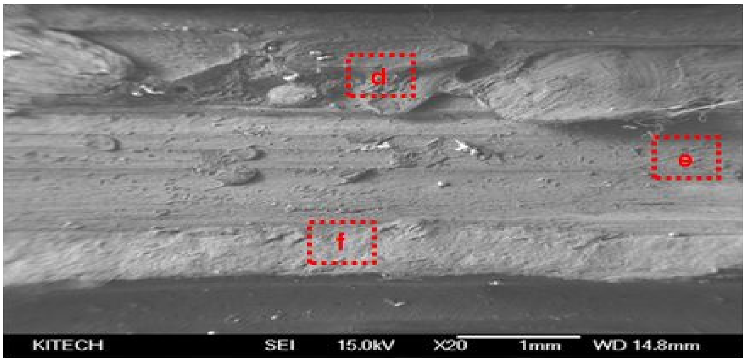

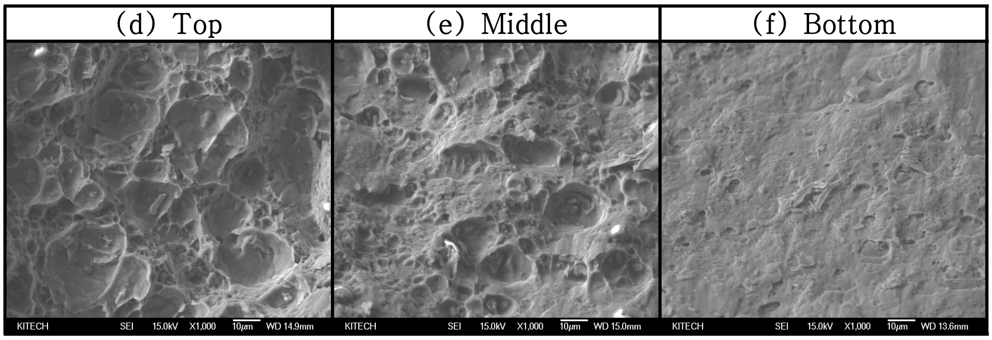

(b)FSW-SS400 side

Fig.4.15 SEM of dissimilar joint by FSW

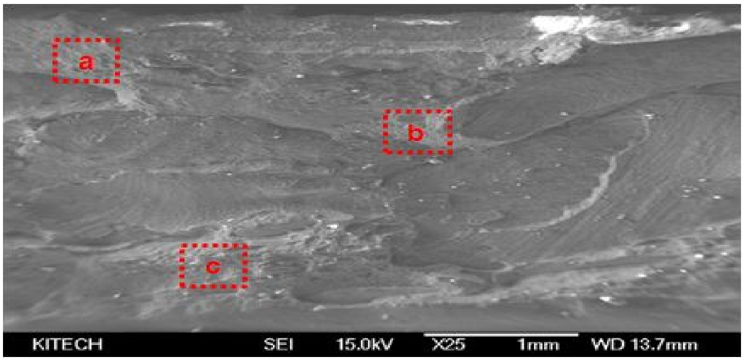

(a) Top

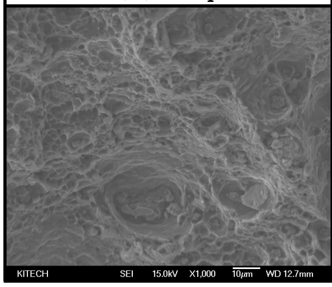

(b) Middle

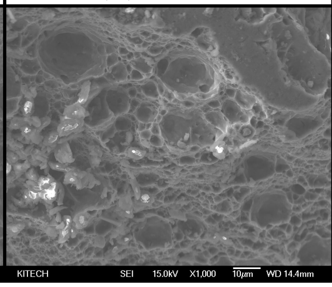

(c) Bottom

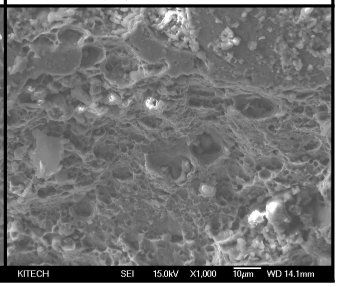

(a)LAFSW– Al6061 side

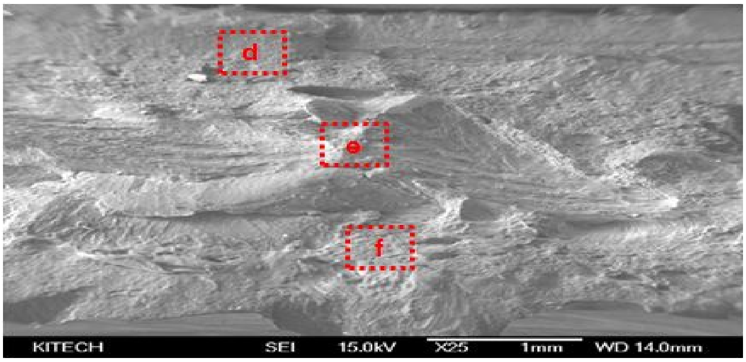

(d) Top

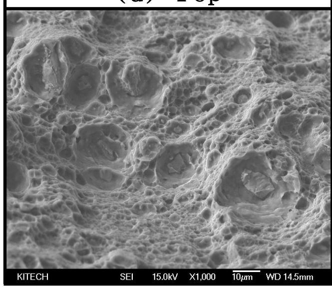

(e) Middle

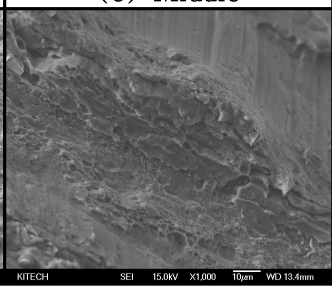

(f) Bottom

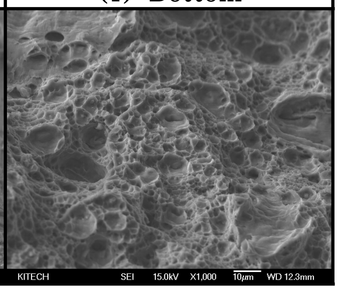

(b)LAFSW–SS400 side

Fig.4.16 SEM of dissimilar joint by LAFSW

4.6.2 SEM and EDS observation of dissimilar joint by LAFSW

The SEM and EDS photographs of the welded joints have been illustrated in Figs 4.17. 4.18 and 4.19 respectively. The possibility of appearing inter-metallic compounds in the interface between steel and aluminum is studied from the SEM images. Judging from SEM and EDS analysis, no inter-metallic compounds was observed on the check points. But, previous research works report the possibility of appearing $FeAl_3$ mainly at the upper part of dissimilar joint interface of aluminum and steel. Here, only Wt% of Al and Fe at aluminum side where steel inclusion are found at weld interface has been analysed.

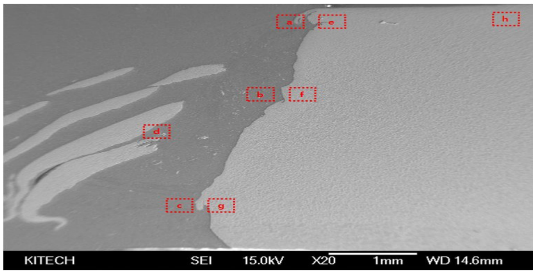

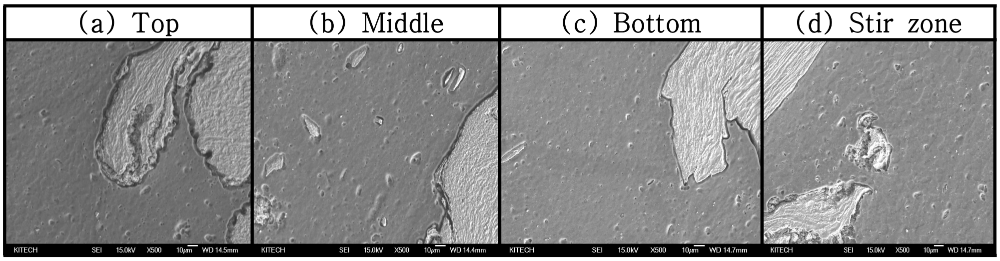

(a)Al6061 side

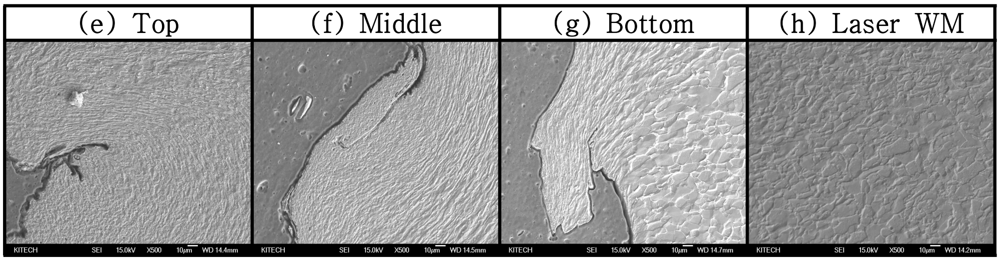

(b)SS400 side

Fig 4.17. SEM of LAFSW

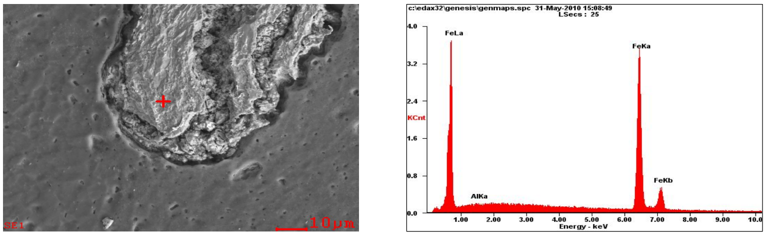

	Wt%	At%
AlK	00.29	00.59
FeK	99.71	99.41
Matrix	Correction	ZAF

(a) Top – Al6061 side

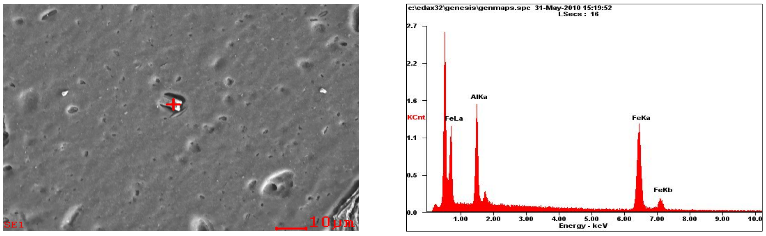

Element	*Wt%*	*At%*
AlK	18.97	32.63
FeK	81.03	67.37
Matrix	Correction	ZAF

(b) Middle – Al6061 side

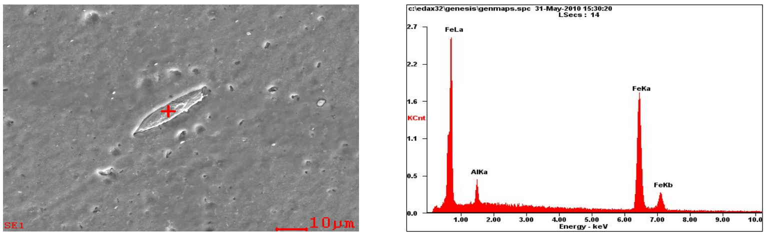

Element	*Wt%*	*At%*
AlK	04.28	08.46
FeK	95.72	91.54
Matrix	Correction	ZAF

(c) Bottom – Al6061 side

Fig 4.18. EDS of Al6061 by LAFSW

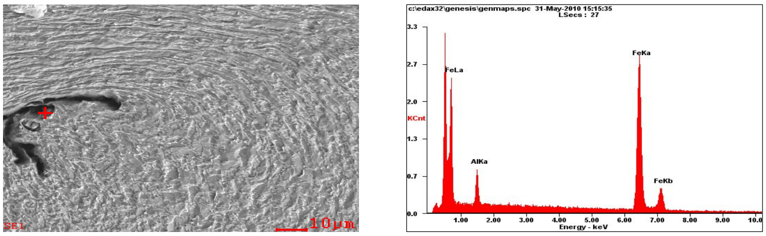

Element	*Wt%*	*At%*
AlK	04.86	09.56
FeK	95.14	90.44
Matrix	Correction	ZAF

(a) Top – SS400 side

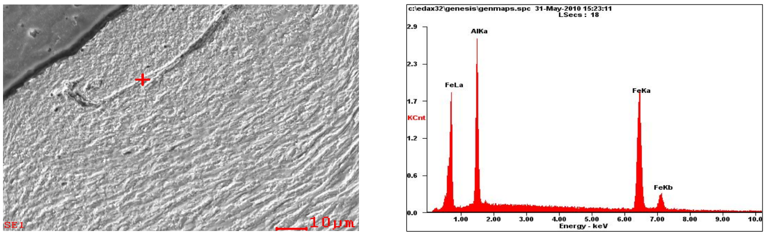

Element	*Wt%*	*At%*
AlK	21.66	36.39
FeK	78.34	63.61
Matrix	Correction	ZAF

(b) Middle – SS400 side

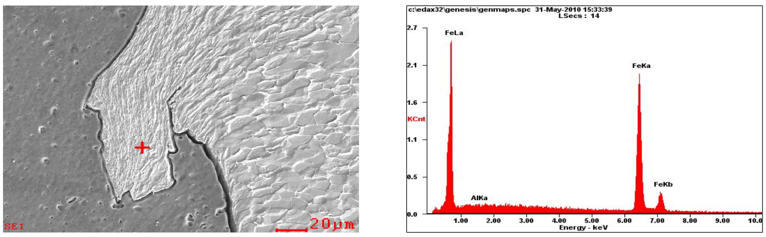

Element	*Wt%*	*At%*
AlK	00.22	00.45
FeK	99.78	99.55
Matrix	Correction	ZAF

(c) Bottom – SS400 side

Fig 4.19. EDS of SS400 by LAFSW

Chapter 5

CONCLUSION

Laser assisted FSW was successfully carried out to join dissimilar materials (Al6061-T6 and SS400). Numerical analysis using 2D model was carried out to simulate the heat distribution characteristics of dissimilar joint. Welding Experiments by FSW and LAFSW were carried out and in order to check the weldability, tensile test, hardness test, and microstructure analysis were carried out with dissimilar weld joint.

From this study following conclusions were made:

1) From numerical analysis results following observations were made:

- The cooling time of Al6061 is higher than SS400 for FSW and LAFSW because of high heat conductivity of Al6061.
- The cooling rate is lower at tool bottom than at shoulder bottom and tool surface because of the difference in heat affected area in both welding process.
- At steel side in LAFSW, the maximum temperature is found at laser affected area during the commencement of welding and temperature is found decreasing from frictional surface towards base metal at shoulder bottom side.
- The difference in temperature as time passes at a point in FSW is more than that in LAFSW at shoulder bottom. From this it is understood that the heat is conducted more to Al6061 by additional laser preheating and thus the cooling takes place slowly in LAFSW .

2) At a tool rotation speed of 400rpm and welding speed 1.4mm/sec, sound dissimilar weld joint having good tensile strength was obtained by LAFSW. But comparing with FSW, overall welding experimental results of LAFSW it is evident that sound weld can be made at higher welding speeds.

3) The tensile strength of FSW dissimilar joint is found to be lower than that of LAFSW at optimum welding conditions. The maximum tensile strength obtained was 315.6MPa and 340MPa for FSW and LAFSW respectively.

3) Due to increase in plastic flow and formation of finer recrystallized grains at the TMAZ and SZ by laser preheating in LAFSW, the hardness values are more in LAFSW compared to FSW.

4) From the microstructure analysis, smaller grain size were observed and parent metal elongated grains were deformed in same direction around the nugget zone in TMAZ of Al6061-T6 by LAFSW compared to FSW. At nugget zone, coarse grain size is appeared in LAFSW when compared to FSW because of more plastic flow due to laser preheating effect. Refined ferrite-bainite microstructure is formed at weld nugget of SS400.

5) From SEM image observation of fractured face of the specimen by FSW and LAFSW, dimple pattern with ductile and brittle fracture was found to occur at joint interface. But more brittle fracture is found in FSW welded specimens. In LAFSW dissimilar joint ductile mode of fracture is found to occur at Al6061 side with fewer brittle particles. Mixed mode of cleavage area and ductile fracture was observed at SS400 side.

The possibility of appearing inter-metallic compounds in the interface between steel and aluminum is studied from the cross sectional SEM and EDS images.

REFERENCES

[1] H.S. Bang, H.S. Bang, S.M. Joo, "Numerical simulation of Al-SPCC weldment", Key Engineering Materials, P1738~1744, Oct., 2006

[2] H Schmidt, J Hattel, J Wert "An analytical model for the heat generation in friction stir welding" Modellign Simul. Mater. Sci. Eng. 10(2004) P.143~157

[3] C. Hamilton, S. Dymek, A. Sommers "A thermal model of Friction stir welding in aluminum alloys" International Jourmal of Machine Tools & Manufacture (2008) P. 1120~1130

[4] Hidetoshi Fujii, Takahiro Tatsuno, Takuya Tsumura " Hybrid Friction Stir Welding of Carbon Steel" Material Science Forum Vols.580-582 (2008) P.393~396

[5] Y.J.Chao, and X.Qi: Heat transfer and thermo-mechanical analysis of Friction Stir joining of Al6061-T6 plates, 1st International Symposium on Friction Stir Welding, (1999).

[6] A.Askari, S.Silling, B.London, and M.Mahoney: Modelling and Analysis of Friction Stir Welding Processes, Friction stir welding and Processing, TMS publication,(2001) p.43.

[7] A.William, Using Gleeble flow stress data to establish optimum FSW processing parameter in Aluminium Alloys, Advanced material processing centre, (2002).

[8] H.S. Bang. "Study on The Mechanical Behaviour of Welded part in thick Plate - Three-dimensional Thermal Elasto-Plastic Analysis Baseon Finite Element Method." Journal of the Korean Welding Society, Vol.10, No.4, pp.37~43, December 1992.

[9] Rajesh S.R., "Development of mathematical model for Thermo - mechanical behavior of Friction Stir Welding an introduction Soldering by using FEM/BEM", 2007

[10] W.B. Lee, S.B. Jung, Gehard Biallas, Martin Schmuecker. "Joint

properties and Interface Analysis of Friction Stir Welded Dissimilar Materials between Austenite Stainless Steel and 6013 Al Alloy" Journal of the Korean Welding Society, Vo.23, No.5, pp.469 ~476, October 2005.

[11] H. Kokawa, S.H.C. Park, Y.S. Sato, K. Okamoto, S. Hirano, M. Inagaki : Microstructures in Friction Stir Welded 304 Austenitic Stainless Steel, Welding in the World, 49(3/4), 2005, pp.34-40

[12] T.J. Lienert, W.L. Steelwag, Jr., B.B Grimmett, and R.W. Warke : Friction Stir Welding Studies on Mild Steel, Welding Journal, 82(1), 2003, pp.1S-9S

[13] AWS, WELDING HANDBOOK, Vol.1, Eighth Edition, 1987.

[14] AWS, WELDING HANDBOOK, Vol.2, Eighth Edition, 1991.

[15] W.M. Thomas, P.L.Threadgill, and E.D. Nicholas : Feasible of Friction Stir Welding Steel, Science and Technology of Welding and Joining, 4(6), 1999, pp. 365-372

[16] L.E.Murr, et al.: Solid-state flow association with the friction stir welding of dissmilar metals, Fluid flow phenomena in metals processing (1999), 31-40

[17] Huseyin Uzun, Claudio Dalle Donne, Alberto Argagnotto, Tommaso Ghidini, Carla Gambaro.:Friction stir welding of dissimilar Al 6013-T4 To X5CrNi18-10 stainless steel, Materials and Design 26 (2005) 41-.46

[18] Z. Sun, R. Karppi, "The application of electron beam welding for the joining of dissimilar metals: an overview", Journal of materials processing technology 59 (1996) 257-267

[19] H.S. Bang, G.Y. Han, "The plane-deformation thermal elasto -plastic analysis during welding of plate", The society of naval architects of korea p33~40, Apr.1994

[20] S. Katayama, et al.: Proc.5th Int.Conf.on TRENDS IN WELDING RESEARCH, Georgia, June (1998), pp.467-472.

Acknowledgments

 본 논문이 완성되기 전까지 부족함이 많은 제자를 세심한 관심과 배려로 항상 저에게 끊임없는 지도와 사랑으로 이끌어주시며, 좋은 말씀과 조언을 아끼지 않았던 방한서 교수님께 진심으로 머리 숙여 감사드립니다,

 또한 지도와 관심을 베풀어주신 방희선 교수님과 이창우 박사님, 신찬호 박사님께 감사의 마음을 전합니다. 그리고 학문에 대한 이해와 애정 어린 지도를 해 주시며 도움을 주신 선박해양공학과의 모든 교수님들께도 감사드립니다.

 지난 2년이 넘는 시간동안 함께 생활하며 서로에게 용기와 격려를 아끼지 않고 학문의 길을 걸었던 저의 연구실 동료들에게 고마운 마음을 전합니다. 졸업논문을 같이 준비하며 실험했던 정미 누나, 영문논문에 많은 조언을 해준 비죠이형, 실험준비 및 수행에 많은 조언을 해준 근홍이형, 준형이형, 멀리 떨어져 있지만 항상 따뜻한 말과 조언을 아끼지 않았던 세민이형, 늦은 밤 항상 같이 자리를 지켜준 용혁이형, 레이저실험에 많은 도움을 준 계성이형, 인장실험 및 경도 측정 하느라 많이 고생한 두송이, 비록 함께 같이 있지는 못하지만 SEM 촬영과 항상 많은 도움을 주었던 기상이, 요트사업 부터 어려운 일이 생기면 항상 도와준 현종이, 폴리싱 및 경도 측정하느라 새벽까지 도와준 정한이, 여러 가지로 많이 도움을 주었던 주현이 이 모든 연구실 사람들에게 감사에 말을 드립니다.

 부족한 자식 공부하는데 부족함이 없이 키워주고 믿어주신 아버지, 어머니, 항상 많은 관심과 사랑을 주신 외할아버지, 외할머니, 이모부, 이모, 곁에서 항상 형을 믿고 따라 주었던 형수 그리고 학교 공부하느라 함께 있어주지 못해도 항상 큰 힘과 믿음을 주었던 은애에게 이 모든 감사의 말을 전하며 이 논문을 마칩니다.

저작물 이용 허락서

학 과	선박해양공학과	학 번	20097096	과 정	석사
성 명	한글: 김현수 한문 : 金顯洙 영문 : Hyun-Su Kim				
주 소	광주광역시 북구문흥동 대주아파트 302동 101호				
연락처	E-MAIL : coolkhs3076@naver.com				
논문제목	한글 : Laser-FSW Hybrid 접합기술을 적용한 이종재료 (Al6061/SS400) 접합부의 접합성 및 기계적 특성에 관한 연구 영어 : A Study on the Weldability and Mechanical Characteristics of Dissimilar Butt Joint by Laser Assisted Friction Stir Welding				

본인이 저작한 위의 저작물에 대하여 다음과 같은 조건아래 조선대학교가 저작물을 이용할 수 있도록 허락하고 동의합니다.

\- 다 음 -

1. 저작물의 DB구축 및 인터넷을 포함한 정보통신망에의 공개를 위한 저작물의 복제, 기억장치에의 저장, 전송 등을 허락함
2. 위의 목적을 위하여 필요한 범위 내에서의 편집・형식상의 변경을 허락함. 다만, 저작물의 내용변경은 금지함.
3. 배포・전송된 저작물의 영리적 목적을 위한 복제, 저장, 전송 등은 금지함.
4. 저작물에 대한 이용기간은 5년으로 하고, 기간종료 3개월 이내에 별도의 의사 표시가 없을 경우에는 저작물의 이용기간을 계속 연장함.
5. 해당 저작물의 저작권을 타인에게 양도하거나 또는 출판을 허락을 하였을 경우에는 1개월 이내에 대학에 이를 통보함.
6. 조선대학교는 저작물의 이용허락 이후 해당 저작물로 인하여 발생하는 타인에 의한 권리 침해에 대하여 일체의 법적 책임을 지지 않음
7. 소속대학의 협정기관에 저작물의 제공 및 인터넷 등 정보통신망을 이용한 저작물의 전송・출력을 허락함.

동의여부 : 동의(O) 반대( )

2010 년 6 월

저작자: 김 현 수 (서명 또는 인)

조선대학교 총장 귀하